

# Robust Two-Layer Partition Clustering of Sparse Multivariate Functional Data

Zhuo Qu<sup>1</sup>, Wenlin Dai<sup>2</sup> and Marc G. Genton<sup>1</sup>

April 27, 2022

## Abstract

In this work, a novel elastic time distance for sparse multivariate functional data is proposed. This concept serves as the foundation for clustering functional data with various time measurements per subject. Subsequently, a robust two-layer partition clustering is introduced. With the proposed distance, our approach not only is applicable to both complete and imbalanced multivariate functional data but also is resistant to outliers and capable of detecting outliers that do not belong to any clusters. The classical distance-based clustering methods such as K-medoids and agglomerative hierarchical clustering are extended to the sparse multivariate functional case based on our proposed distance. Numerical experiments on the simulated data highlight that the performance of the proposed algorithm is superior to the performances of the existing model-based and extended distance-based methods. Using Northwest Pacific cyclone track data as an example, we demonstrate the effectiveness of the proposed approach. The code is available [online](#) for readers to apply our clustering method and replicate our analyses.

**Some key words:** Cyclone data, Elastic time distance, Imbalanced data, Multivariate functional data, Outliers, Robust clustering

---

<sup>1</sup>Statistics Program, King Abdullah University of Science and Technology, Thuwal 23955-6900, Saudi Arabia. E-mail: zhuo.qu@kaust.edu.sa, marc.genton@kaust.edu.sa

This research was supported by the King Abdullah University of Science and Technology (KAUST).

<sup>2</sup>Institute of Statistics and Big Data, Renmin University of China, Beijing 100872, China. E-mail: wenlin.dai@ruc.edu.cn

# 1 Introduction

Functional data analysis (FDA, [Ramsay & Silverman 2005](#)) is a branch of statistics that analyzes observations that can be regarded as curves, surfaces, or any object evolving over a continuum. It has wide applications in many fields, such as meteorology, medicine, finance, biology, and language. The real-life examples of the applications of FDA are the analyses of typhoon trajectories ([Misumi et al. 2019](#)), teletransmitted electrocardiograph (ECG) traces ([Ieva et al. 2011](#)), stock share prices over time ([Horváth & Kokoszka 2012](#)), growth curves of different body parts ([Sheehy et al. 2000](#)), CD4 level counts ([Yao et al. 2005](#)), and character handwritings ([Kneip et al. 2000](#)). With the advances in data collection techniques, huge amounts of functional data are being recorded for various purposes and these data usually show heterogeneity. Hence, clustering these functional observations into homogeneous subgroups is crucial.

Overall, functional clustering can be achieved using four types of methods, according to [Jacques & Preda \(2014a\)](#): 1) the raw data methods that involve clustering directly the curves on their finite set of points—for example, the piecewise constant nonparametric density estimation by [Boullé \(2012\)](#); 2) the filtering methods that require smoothing curves into a basis of functions and clustering the resulting expansion coefficients in turn—for example, the principal points of curves ([Tarpey & Kinateder 2003](#)), B-spline fitting ([Abraham et al. 2003](#)), and functional principal component analysis ([Peng & Müller 2008](#)); 3) the adaptive methods that perform the simultaneous clustering and expression of the curves into a finite dimensional space—for example, basis expansion coefficients modelling ([James & Sugar 2003](#), [Samé et al. 2011](#), [Giacofci et al. 2013](#)), and functional principal component analysis ([Chiou & Li 2007](#), [Bouveyron & Jacques 2011](#), [Jacques & Preda 2013](#), [Jacques & Preda 2014b](#), [Centofanti et al. 2021](#)); and 4) the distance-based methods where usual clustering algorithms are applied with specific distances for functional data—for example, the approaches reported by [Ferraty & Vieu \(2006\)](#), [Cuesta-Albertos & Fraiman \(2007\)](#), [Ieva et al. \(2011\)](#), [Liu et al. \(2012\)](#), [Antoniadis et al. \(2013\)](#), and [García et al. \(2015\)](#). Although the clustering method in [Centofanti et al. \(2021\)](#) can be applied

to an irregular time grid, there may be computation issues due to the estimation of parameter sets in big functional data clustering. Given new distance measures, classical clustering methods have been extended to the functional framework. For example, a hierarchical clustering algorithm (Olson 1995) was considered by Liu et al. (2012); the  $K$ -means algorithm (Hartigan & Wong 1979) was recommended by Antoniadis et al. (2013) and García et al. (2015); and the  $K$ -medoids method (Kaufman & Rousseeuw 1990, Al Abid 2014), which is a modification of the  $K$ -means method, was developed by Chen et al. (2017). In addition, Floriello & Vitelli (2017) extended the  $K$ -means,  $K$ -medoids, and hierarchical clustering algorithms to sparse multivariate and functional frameworks.

However, for multivariate functional data, few innovations exist for data clustering. From the viewpoint of generalization of adaptive methods, Jacques & Preda (2014b) generalized functional clustering from univariate to multivariate functional data via multivariate functional principal component analysis (MFPCA, Ramsay & Silverman). Furthermore, Schmutz et al. (2020) extended the work of Jacques & Preda (2014b), and their new method (FunHDDC) is advantageous from two perspectives: for modelling all principal component scores whose estimated variances are non-null and for using the expectation-maximization (EM) algorithm to propose a criterion for selecting the number of clusters. Moreover, Misumi et al. (2019) proposed a multivariate nonlinear mixed-effects model to express multivariate functional data and applied a nonhierarchical clustering algorithm based on self-organizing maps to the predicted coefficient vectors of individual-specific random effect functions. With regard to the distance methods, Ieva et al. (2013) generalized the distance measure to multivariate functional data and presented an analysis of teletransmitted ECG traces, and Meng et al. (2018) proposed a new distance and applied the  $K$ -means clustering algorithm to multivariate functional data. Other methods considered clustering curves while capturing the features of amplitude or phase variations. For instance, Sangalli et al. (2010) proposed a  $K$ -means clustering method to decompose amplitude and phase variations while assuming a linear warping time function; Park & Ahn (2017) proposed a condi-

tional subject-specific warping framework and considered multivariate functional clustering with phase variation.

For methods with a given number of clusters, the criteria to find the optimal number of clusters, i.e.,  $K$ , are provided by  $K$ -means clustering (Kodinariya & Makwana 2013), and agglomerative hierarchical clustering (Jung et al. 2003, Zhou et al. 2016, and Zambelli 2016). Generally, the optimal  $K$  can be determined from the elbow value (Shi et al. 2021), average silhouette (Struyf et al. 1997, Batool & Hennig 2021), gap statistics (Tibshirani et al. 2001), model-based Akaike Information Criterion (AIC, Akaike 1974), Bayesian Information Criterion (BIC, Schwarz 1978), and integrated classification likelihood (Biernacki et al. 2000).

Before discussing the features of the existing methods, we note that sparse (or imbalanced) multivariate functional data are common in practice. We define the sparse (multivariate) functional data as data objects with various time grids per subject. The imbalanced (multivariate) functional data are the data objects such that some objects may have a large number of measurements while others may have few measurements. Here, we assume that the measurement is either observed or missing for all variables and do not consider the case where the measurements for one index are observed for some variables but missing for others. Two main characteristics are observed for the existing clustering methods: first, for imbalanced multivariate functional data, no specific distance measurements are defined and the model-based clustering methods, except for that of Misumi et al. (2019), cannot be applied directly; second, the above methods rarely consider outliers, though real data are often corrupted by noises and outliers, see Ronchetti (2021) for a recent review. Although some improvements have been achieved in  $K$ -means clustering (Wang & Su 2011) and hierarchical clustering (Gagolewski et al. 2016) for multivariate data to reduce the influence of outliers, robust (i.e., outlier-resistant) clustering algorithms for sparse multivariate functional data are lacking.

The objective of this work is to develop an outlier-resistant clustering method for imbalanced multivariate functional data that can have various time grids per subject. First, we propose

the concept of elastic time distance (ETD), which is applicable to (multivariate) functional data with either identical or different time measurements per subject. Second, we propose an outlier-resistant method to detect clusters and outliers based on the ETD measures.

The rest of the paper is organized as follows. Section 2 proposes a novel robust clustering algorithm based on a new distance measure; we introduce the ETD, which can be applied to standard and imbalanced multivariate functional data, and propose two algorithms, namely, a distance-based two-layer partition algorithm and a cluster and outlier recognition algorithm to determine the primary clusters and outliers. We refer to the proposed method as robust two-layer partition (RTLTP) clustering. In Section 3, we describe the numerical experiments performed to evaluate the clustering precision and robustness of our approach and compare these results with those of the existing methods. In Section 4, we present the results of application of our method to Northwest Pacific cyclone track data to establish the efficiency of our method. Section 5 concludes the paper with a summary and discussion. The code is available [online](#) for readers to apply our clustering method and replicate our analyses.

## 2 Multivariate Functional Data Clustering

A multivariate functional random variable of  $p$  dimensions,  $\mathbf{Y} = (Y^{(1)}, \dots, Y^{(p)})^\top$ , is a  $p$ -variate random vector with values in an infinite-dimensional space. In a well-known model of multivariate functional data ([Hsing & Eubank 2015](#)), the data are considered as sample paths of a stochastic process  $\mathbf{Y} = \{\mathbf{Y}(t) := (Y^{(1)}(t), \dots, Y^{(p)}(t))^\top\}_{t \in \mathcal{T}}$  taking values in some Hilbert space,  $\mathcal{H}$ , of functions defined on some set  $\mathcal{T}$ . Generally,  $\mathcal{H}$  is restricted to be a space of  $\mathbb{R}^p$ -valued functions, and  $\mathcal{T}$  is a subset of  $\mathbb{R}$ , representing a time, wavelength, or another index. Then, the multivariate functional data represent a set  $S := \{\mathbf{Y}_1, \dots, \mathbf{Y}_N\}$  of observations of  $\mathbf{Y}$ .

Although the observations are supposed to be infinite-dimensional, in practice, we only have discrete observations  $\mathbf{Y}_{n,k}$  ( $n = 1, \dots, N$ ) of each sample path  $\mathbf{Y}_n$  evaluated at the  $k$ th ( $k = 1, \dots, T_n$ ) knot of the set  $\mathbf{t}_n = \{t_{n,k}, k = 1, \dots, T_n\}$ . Hence, without loss of generality, we assume

$\mathcal{T}$  to be the interval  $[0, 1]$ , and both the number and locations of measurements can vary per subject.

## 2.1 Elastic Time Distance

We first introduce the concept of elastic time distance (ETD), which measures the distances between observations under the setting described in the previous paragraph. ETD can be obtained in three steps: building a standard equidistant time grid for all curves, transforming the original curves into aligned curves, and choosing the maximal point-wise  $L^2$  norm (Adams & Fournier 2003) over the standard grid. We define the standard grid from the observation set  $S$  and the corresponding aligned observation as follows.

*Definition 1* (Standard grid). We define the standard grid  $\mathbf{st}$  as a set  $\{st_k := \frac{k-1}{T-1}, k = 1, \dots, T\}$  with  $T = \max_{n=1}^N T_n$ .

*Definition 2* (Aligned observation). We define the aligned observation  $\tilde{\mathbf{Y}}_n$  as a set  $\{\tilde{\mathbf{Y}}_{n,k} = \mathbf{Y}_n(\tilde{t}_{n,k}), \tilde{t}_{n,k} := \arg \min_{t \in \mathbf{t}_n} |t - st_k|, k = 1, \dots, T\}$ . Here, note that  $\tilde{\mathbf{Y}}_{n,k} = (\tilde{Y}_{n,k}^{(1)}, \dots, \tilde{Y}_{n,k}^{(p)})^\top \in \mathbb{R}^p$ .

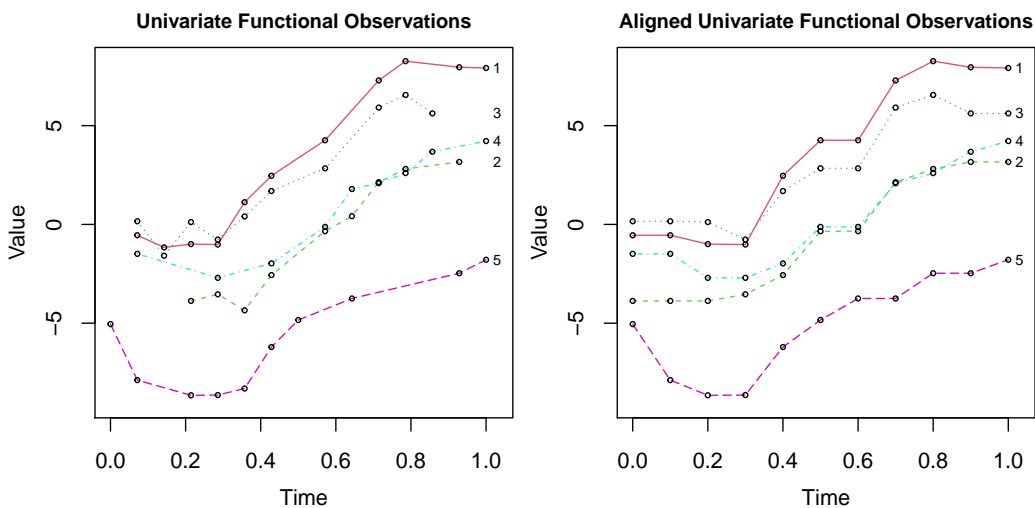


Figure 1: Example of five univariate functional samples evaluated on various time grids (left), and the corresponding aligned univariate functional samples evaluated on the standard grid (right).

As shown in Figure 1, because the maximum number of measurements  $T$  from the five samples  $\{\mathbf{Y}_1, \dots, \mathbf{Y}_5\}$  is 11, we have  $\mathbf{st} = \{k/10, i = 0, \dots, 10\}$ . Then, the observation at any standard time  $st_k$  ( $k = 1, \dots, 11$ ) is the one with the closest time difference from the corresponding time

point in the standard time grid. For example,  $\mathbf{Y}_1$  has 11 measurements at  $\{t_{1,1}, \dots, t_{1,11}\}$ , and we express its aligned observation evaluated at the standard time in the form of  $(st_k, \tilde{\mathbf{Y}}_{1,k})$  as follows:  $(st_1, \mathbf{Y}_{1,1}), (st_2, \mathbf{Y}_{1,1}), (st_3, \mathbf{Y}_{1,3}), (st_4, \mathbf{Y}_{1,4}), (st_5, \mathbf{Y}_{1,6}), (st_6, \mathbf{Y}_{1,7}), (st_7, \mathbf{Y}_{1,7}), (st_8, \mathbf{Y}_{1,8}), (st_9, \mathbf{Y}_{1,9}), (st_{10}, \mathbf{Y}_{1,10})$ , and  $(st_{10}, \mathbf{Y}_{1,11})$ . Although the trend of the aligned observation in an interval is slightly different from the original one (see the different measurements in  $[0.4, 0.6]$  before and after the alignment), the aligned observations provide a simple and feasible framework for calculating the pairwise distance between the observations and measuring the similarity between sparse (multivariate) functional data.

For any  $\mathbf{Y}_n, \mathbf{Y}_m \in S$ , the ETD between  $\mathbf{Y}_n$  and  $\mathbf{Y}_m$  is calculated as follows:

$$ETD(\mathbf{Y}_n, \mathbf{Y}_m) = \max_{k=1, \dots, T} \sqrt{\sum_{d=1}^p (\tilde{Y}_{n,k}^{(d)} - \tilde{Y}_{m,k}^{(d)})^2}, \quad 1 \leq n \leq m \leq N. \quad (1)$$

When all the curves are from common and standard time grids, there is no difference between a functional observation and its aligned version. Then, the ETD becomes the  $L^\infty$  norm (Horn & Johnson 1990) of a  $T$ -dimensional vector, where each element of the vector is a Euclidean distance (Tabak 2014 p.150) for  $p$ -dimensional points. We prove that  $ETD(\mathbf{Y}_n, \mathbf{Y}_m)$  is a semimetric (Collatz 1966) that satisfies the properties described in Theorem 1.

**Theorem 1** *ETD, as a semimetric, is a distance function such that  $\forall \mathbf{Y}_n, \mathbf{Y}_m, \mathbf{Y}_l \in S$ :*

1. *Non-negativity:  $ETD(\mathbf{Y}_n, \mathbf{Y}_m) \geq 0$ .*
2. *Zero for identical curves:  $ETD(\mathbf{Y}_n, \mathbf{Y}_n) = 0$ .*
3. *Symmetry:  $ETD(\mathbf{Y}_n, \mathbf{Y}_m) = ETD(\mathbf{Y}_m, \mathbf{Y}_n)$ .*
4. *Triangular inequality:  $ETD(\mathbf{Y}_n, \mathbf{Y}_m) \leq ETD(\mathbf{Y}_n, \mathbf{Y}_l) + ETD(\mathbf{Y}_l, \mathbf{Y}_m)$ .*

**Proof:** 1.  $ETD(\mathbf{Y}_n, \mathbf{Y}_m) \geq 0$  from (1).

2.  $ETD(\mathbf{Y}_n, \mathbf{Y}_n) = 0$  from (1). Unlike a metric space (Choudhary 1993), points in a semi-metric space need not be distinguishable; that is, one may have  $ETD(\mathbf{Y}_n, \mathbf{Y}_m) = 0$  for distinct  $\mathbf{Y}_n$  and  $\mathbf{Y}_m$ . If  $ETD(\mathbf{Y}_n, \mathbf{Y}_m) = 0$ , then we have  $\tilde{\mathbf{Y}}_n = \tilde{\mathbf{Y}}_m$ , but the original functions  $\mathbf{Y}_n$  and  $\mathbf{Y}_m$  may vary in terms of the location and number of measurement grids.

3.  $ETD(\mathbf{Y}_n, \mathbf{Y}_m) = ETD(\mathbf{Y}_m, \mathbf{Y}_n)$  from (1).

4. Given  $\sum_{d=1}^p (\tilde{Y}_{n,k}^{(d)} - \tilde{Y}_{m,k}^{(d)})^2 = \sum_{d=1}^p (\tilde{Y}_{n,k}^{(d)} - \tilde{Y}_{l,k}^{(d)} + \tilde{Y}_{l,k}^{(d)} - \tilde{Y}_{m,k}^{(d)})^2 = \sum_{d=1}^p (\tilde{Y}_{n,k}^{(d)} - \tilde{Y}_{l,k}^{(d)})^2 + \sum_{d=1}^p (\tilde{Y}_{l,k}^{(d)} - \tilde{Y}_{m,k}^{(d)})^2 + \sum_{d=1}^p 2(\tilde{Y}_{n,k}^{(d)} - \tilde{Y}_{l,k}^{(d)})(\tilde{Y}_{l,k}^{(d)} - \tilde{Y}_{m,k}^{(d)}) \forall k = 1, \dots, T$  and  $\sum_{d=1}^p (\tilde{Y}_{n,k}^{(d)} - \tilde{Y}_{l,k}^{(d)})(\tilde{Y}_{l,k}^{(d)} - \tilde{Y}_{m,k}^{(d)}) \leq \sum_{d=1}^p |\tilde{Y}_{n,k}^{(d)} - \tilde{Y}_{l,k}^{(d)}| \cdot \sum_{d=1}^p |\tilde{Y}_{l,k}^{(d)} - \tilde{Y}_{m,k}^{(d)}|$ , we have  $\sum_{d=1}^p (\tilde{Y}_{n,k}^{(d)} - \tilde{Y}_{m,k}^{(d)})^2 \leq (\sum_{d=1}^p |\tilde{Y}_{n,k}^{(d)} - \tilde{Y}_{l,k}^{(d)}| + \sum_{d=1}^p |\tilde{Y}_{l,k}^{(d)} - \tilde{Y}_{m,k}^{(d)}|)^2$ . This is equivalent to  $\sqrt{\sum_{d=1}^p (\tilde{Y}_{n,k}^{(d)} - \tilde{Y}_{m,k}^{(d)})^2} \leq \sqrt{\sum_{d=1}^p (\tilde{Y}_{n,k}^{(d)} - \tilde{Y}_{l,k}^{(d)})^2} + \sqrt{\sum_{d=1}^p (\tilde{Y}_{l,k}^{(d)} - \tilde{Y}_{m,k}^{(d)})^2}$ . The inequality holds after taking the maximum. By combining the inequality relation with (1), we obtain that  $ETD(\mathbf{Y}_n, \mathbf{Y}_m) \leq ETD(\mathbf{Y}_n, \mathbf{Y}_l) + ETD(\mathbf{Y}_l, \mathbf{Y}_m)$ .  $\square$

The procedure of calculating ETD in (1) is summarized in Algorithm 1 in the Appendix. Let  $D(S)$  be a set containing the pairwise ETDs between observations in  $S$ . The existing distance-based methods, such as the classical  $K$ -medoids (Kaufman & Rousseeuw 1990) and the agglomerative hierarchical clustering (Nielsen 2016), can be naturally combined with ETD.

## 2.2 Two-Layer Partition Clustering Algorithm

Motivated by the concept of depth-based core neighbours (Jeong et al. 2016), we define the neighbours of each curve and naturally introduce the first-layer partition. However, the output of the first-layer partition may have disjoint sets that are from homogeneous groups. Hence, we implement another layer to make it possible to merge nearby groups into a cluster. In practice, according to our criterion, the third-layer partition leads to one cluster that contains all curves. Hence, we propose a two-layer partition clustering algorithm. Here, before describing the clustering, related concepts are introduced. Let  $|A|$  be the cardinality of the set  $A$ , and  $q_\theta(A)$  be the  $\theta$ -quantile ( $0 < \theta < 1$ ) of the set  $A$ .

*Definition 3* (Neighbours of a curve). The set  $nbr(\mathbf{Y}_n, S) := \{\mathbf{Y}_m : ETD(\mathbf{Y}_n, \mathbf{Y}_m) < q_\theta(D(S)), \forall \mathbf{Y}_n, \mathbf{Y}_m \in S\}$  consists of neighbours of  $\mathbf{Y}_n$  in the set  $S$ . Here,  $\theta$  is used to determine the number of neighbours per curve.

Generally, the number of neighbours per curve is positively correlated to  $\theta$ . Empirically speaking, if  $\theta \geq 0.25$ , then all curves are merged into one group; furthermore, if  $\theta < 0.01$ , then many



clusters do not have neighbours except themselves. The criterion for selecting the optimal  $\theta$  is introduced in Section 2.4.

*Definition 4* (Core and center of the set). For any set  $A$ , its core is the element with the most neighbours, i.e.,  $core(A) = \arg \max_{\mathbf{Y} \in A} |nbr(\mathbf{Y}, A)|$ . If  $A$  is a cluster, we name  $core(A)$  as the center of  $A$ .

*Definition 5* (Disjoint partitions). We define the disjoint partition  $\mathbf{P} = (P_1, \dots, P_L)$  as a separation of  $S$ , where  $L$  is the number of disjoint sets, and  $L \leq N$ .  $\mathbf{P}$  satisfies three conditions:  $P_i \cap P_j = \emptyset$  ( $1 \leq i < j \leq L$ ),  $P_1 \cup \dots \cup P_L = S$ , and  $|P_1| \geq |P_2| \geq \dots \geq |P_L|$ . For a disjoint partition  $\mathbf{P}$ , let  $\mathbf{P}^i$  be the  $i$ -th set in the partition  $\mathbf{P}$ .

The idea of the two-layer partition clustering algorithm is similar to the bottom-up approach (Nielsen 2016) in agglomerative hierarchical clustering. However, we implement only two layers of hierarchy and do not continue until all curves are merged to one cluster. In the first layer, each curve, as an isolated cluster, is merged into disjoint groups based on the concepts of neighbours and the core. Then, in the second layer, the first-layer disjoint groups are merged into a set of clusters. We name the first-layer (group) partition as  $\mathbf{G}$ , and the second-layer (cluster) partition as  $\mathbf{C}$ , and both satisfy *Definition 5*. The criteria for determining the first and second layers of the partitions are proposed as follows.

*Criterion 1* (The first-layer partition  $\mathbf{G}$ ). We obtain the first-layer partition  $\mathbf{G}$  from the core and its neighbours. First, we set the curve with the most neighbours in the observation set  $S$  as a core and define the set consisting of all its neighbours as the first prioritized group  $\mathbf{G}^1$ . Then, we find the curve with the most neighbours in the remaining observations  $S \setminus \mathbf{G}^1$  as a core and define the set consisting of its neighbours in the remaining observations as the second prioritized group  $\mathbf{G}^2$ . Subsequently, we continue the process of finding the core of the remaining observations and defining its neighbours in the remaining observations as a set  $\mathbf{G}^i$  ( $i \geq 3$ ) until all curves are considered. Let  $M$  represent the cardinality of  $\mathbf{G}$ .

For  $\mathbf{G}^i, \mathbf{G}^j \in \mathbf{G}$  ( $1 \leq i < j \leq M$ ) in *Criterion 1*, we have  $|\mathbf{G}^i| \geq |\mathbf{G}^j|$ , where  $\mathbf{G}^i$  is the priori-

tized group, and  $\mathbf{G}^j$  is the subordinate group. The pairwise merging principle  $merge(\mathbf{G}^i, \mathbf{G}^j)$  is as follows: a subordinate group  $\mathbf{G}^j$  may be merged to a prioritized group  $\mathbf{G}^i$  if the core of  $\mathbf{G}^j$  is a neighbour of a curve from  $\mathbf{G}^i$  in  $S$ , and if  $\mathbf{G}^j$  was not merged to any previous prioritized group  $\mathbf{G}^k$  ( $1 \leq k < i$ ) yet.

*Criterion 2* (The second-layer partition  $\mathbf{C}$ ). To obtain the second-layer partition  $\mathbf{C}$ , first, we initialize  $\mathbf{C}^1$  as the most prioritized group in the observation set  $S$ , i.e.,  $\mathbf{G}^1$ . Then, for all subordinate groups of  $\mathbf{C}^1$ ,  $\mathbf{G}^i$  ( $i = 2, \dots, M$ ), we check the pairwise merging principle  $merge(\mathbf{C}^1, \mathbf{G}^i)$  and merge  $\mathbf{G}^i$  with  $\mathbf{C}^1$  ( $\mathbf{C}^1 := \mathbf{C}^1 \cup \mathbf{G}^i$ ) if the principle is satisfied. Next, we continue the following steps: initialize the new cluster  $\mathbf{C}^{j+1}$  ( $j \geq 1$ ) as the most prioritized group in the set remaining to be merged ( $S \setminus (\bigcup_{l=1}^j \mathbf{C}^l)$ ), check the pairwise merging principle between  $\mathbf{C}^{j+1}$  and all its subordinate groups in  $S \setminus (\bigcup_{l=1}^j \mathbf{C}^l)$ , and update  $\mathbf{C}^{j+1}$  accordingly until all curves are in the cluster partition  $\mathbf{C}$ . Finally, we use  $I$  to represent the cardinality of the partition  $\mathbf{C}$ .

Algorithm 2 in the Appendix is used to find the clusters from two layers of hierarchy according to *Definitions 1-5* and *Criteria 1* and *2*.

### 2.3 Cluster and Outlier Recognition Algorithm

The output of Algorithm 2 may include clusters with a large number of curves and some with few curves because of the noise and outliers in the observations. To solve this issue, we propose Algorithm 3 for recognizing the primary clusters and outliers using  $p_m$  and  $\alpha$ . Here,  $p_m$  denotes the minimum proportion of the size of a cluster divided by the sample size, and  $\alpha$  ( $0 < \alpha < 1$ ) is the threshold that defines the  $\alpha$ -quantile of the distances between curves inside a cluster and the cluster center. Let  $d_x(A)$  be the empirical cumulative distribution of  $x$  in the set  $A$ . The criterion for selecting the primary clusters and outliers is proposed as follows.

*Criterion 3* (The primary cluster set and outliers). We first initialize the primary cluster sets  $\mathbf{C}_p = \{\mathbf{C}^i \text{ if } |\mathbf{C}^i| \geq Np_m, i = 1, \dots, I\}$ . Hence, each set in  $\mathbf{C}_p$  contains at least  $Np_m$  number of curves. Naturally, the potential outlier set is  $O_p = \{\mathbf{X} \in \mathbf{C}^i \text{ if } |\mathbf{C}^i| < Np_m \forall i = 1, \dots, I\}$ .

Let the outlier set be  $O$ . The potential outlier  $\mathbf{X} \in O_p$  is labeled as an outlier ( $\mathbf{X} \in O$ ), if for any  $C \in \mathbf{C}_p$ , the ETD between  $\mathbf{X}$  and  $core(C)$  is larger than the  $\alpha$ -quantile of the set  $D(C, core(C))$ , which is the set of the ETD between each element in  $C$  and  $core(C)$ . Otherwise,  $\mathbf{X}$  is classified into  $\mathbf{C}^i$  in  $\mathbf{C}_p$  if  $\mathbf{C}^i = \arg \min_{C \in \mathbf{C}_p} d_{ETD(\mathbf{X}, core(C))}(D(C, core(C)))$ . In a mathematical notation,  $\forall \mathbf{X} \in O_p$ ,

$$\mathbf{X} \in \begin{cases} O, & \text{if } ETD(\mathbf{X}, core(C)) > q_\alpha(D(C, core(C))) \forall C \in \mathbf{C}_p, \\ \mathbf{C}^i, & \text{if } \mathbf{C}^i := \arg \min_{C \in \mathbf{C}_p} d_{ETD(\mathbf{X}, core(C))}(D(C, core(C))). \end{cases}$$

Algorithm 3 in the Appendix, applies *Criterion 3* and obtains a set of primary clusters  $\mathbf{C}_p$  and outliers  $O$ . We find that the clustering results are quite stable when  $p_m \leq 0.05$ , and  $0.85 \leq \alpha \leq 0.9$  according to the simulations yet to be reported. Hence, we recommend  $p_m = 0.05$ , and  $\alpha$  any value between 0.85 and 0.9. Adoption of Algorithm 3 makes the two-layer partition clustering (Algorithm 2) robust to outliers, and we name this method as RTLTP clustering.

## 2.4 Clustering Execution

The final results  $\mathbf{C}_p$  and  $O$  obtained from Algorithm 3 may differ if we apply various  $\theta$ . Thus, we first select the optimal  $\theta$ . Thereafter, we adopt  $\mathbf{C}_p$  and  $O$  under the optimal  $\theta$ . The optimal  $\theta$  is the one with the largest average silhouette value (Batool & Hennig 2021). For  $\theta \in [0.01, 0.3]$ , after obtaining a set of primary clusters  $\mathbf{C}_{p,\theta} = (\mathbf{C}_{p,\theta}^1, \dots, \mathbf{C}_{p,\theta}^{B_\theta})$  and outliers  $O_\theta$ , we apply the average silhouette value to assess the goodness of clustering, which is the mean of the silhouette values of all data objects. The original silhouette value (Rousseeuw 1987) is only defined when the object  $\mathbf{Y}_k$  belongs to a cluster  $\mathbf{C}_{p,\theta}^b$  ( $1 \leq b \leq B_\theta$ ). Here, we add the definition of the silhouette value when the object is in the outlier set  $O_\theta$ . If  $\mathbf{Y}_k \in \mathbf{C}_{p,\theta}^b$ , then  $a(\theta, \mathbf{Y}_k) = \frac{1}{|\mathbf{C}_{p,\theta}^b| - 1} \sum_{\substack{l \neq k \\ \mathbf{Y}_l \in \mathbf{C}_{p,\theta}^b}} ETD(\mathbf{Y}_k, \mathbf{Y}_l)$ ,  $b(\theta, \mathbf{Y}_k) = \min_{\substack{c \neq b \\ 1 \leq c \leq B_\theta}} \frac{1}{|\mathbf{C}_{p,\theta}^c|} \sum_{\mathbf{Y}_l \in \mathbf{C}_{p,\theta}^c} ETD(\mathbf{Y}_k, \mathbf{Y}_l)$ , and the silhouette value of  $\mathbf{Y}_k$  is  $s(\theta, \mathbf{Y}_k) = \frac{b(\theta, \mathbf{Y}_k) - a(\theta, \mathbf{Y}_k)}{\max\{a(\theta, \mathbf{Y}_k), b(\theta, \mathbf{Y}_k)\}}$ . If  $\mathbf{Y}_k \in O_\theta$ , then let  $s(\theta, \mathbf{Y}_k) = 0$ . The optimal  $\theta$  is defined as  $\theta = \arg \max_{\theta \in [0.01, 0.3]} \bar{s}(\theta)$ , with the average silhouette value  $\bar{s}(\theta) = \frac{1}{N} \sum_{k=1}^N s(\theta, \mathbf{Y}_k)$ . The

silhouette value measures the resemblance of an object to its cluster compared to other clusters and ranges from  $-1$  to  $1$ . Here, a high value means that the object is well matched to its cohesion and poorly matched to neighbouring clusters, and a low value indicates that the clustering configuration may have an inappropriate number of clusters.

Principally, any distance measures suitable for multivariate functional data can be used in the RTLP clustering. We use ETD as a building block as it is applicable for both complete and imbalanced multivariate functional data. Overall, the RTLP clustering is executed in several steps:

- 1) Compute ETD according to Algorithm 1.
- 2) Execute Algorithms 2-3 for  $\theta \in [0.01, 0.3]$  and compute the average silhouette value  $\bar{s}(\theta)$ .

The optimal  $\theta$  is the one with the highest  $\bar{s}(\theta)$ .

- 3) Implement Algorithms 2-3 under the optimal  $\theta$  from 2), and obtain the set of primary clusters  $\mathbf{C}_p$  and outliers  $O$ .

To illustrate the application of RTLP, we present the stepwise results for a clustering scenario. As shown in Figure 2 (a), we generated 120 curves, and four clusters with a cardinality of 30. Subsequently, we generated 12 outliers out of 120 curves which are marked in dashed red. Then, we make 96 out of 120 curves contain missing values. Here, the standard time grid has 20 equidistant points from 0 to 1. For the curves with missing values, six values are missing randomly in the standard time grid on average, and the locations of the missing measurements are independent and random per subject. The transparency of the color increases with the time elapsed.

After calculating the ETD of the above samples, we execute Algorithms 2-3 under the conditions of  $p_m = 0.05$ ,  $\alpha = 0.87$  and  $\theta \in [0.01, 0.3]$ . Figure 2 (b) indicates an increase in  $\bar{s}(\theta)$  for  $\theta < 0.08$  when there are more than four clusters; a stable  $\bar{s}(\theta)$  for  $0.08 \leq \theta \leq 0.21$ , corresponding to the correct number of clusters with a slight movement of the outliers; and a decrease in  $\bar{s}(\theta)$ , when there are less than four clusters. We see that the optimal  $\theta$  is 0.08, corresponding to the

highest average silhouette value. Subsequently, we implement Algorithms 2-3 under the condition that  $\theta = 0.08$ . Figures 2 (c) and (d) show the results of the first- and second-layer partitions, i.e.,  $\mathbf{G}$  and  $\mathbf{C}$ , respectively, from Algorithm 2. The first four sets in  $\mathbf{G}$  and  $\mathbf{C}$  merge the majority of the curves and are successively marked in black, red, green, and blue. The remaining sets in  $\mathbf{G}$  and  $\mathbf{C}$  have a cardinality of either one or two with other distinct colors per set. Figures 2 (e) and (f) show identical results obtained before and after updating the primary clusters  $\mathbf{C}_p$  via Algorithm 3. On applying *Criterion 3*, all potential outliers remain as outliers. Finally, we detected 12 outliers, and all true outliers were correctly detected, as seen in Figure 2 (f).

Algorithm 1 regards  $ETD(\mathbf{Y}_i, \mathbf{Y}_j)$  as the basic operation. Algorithm 2 regards  $\mathbf{G}^M \leftarrow nbr(core(\tilde{S}_M), \tilde{S}_M)$  as the basic operation. For Algorithm 3,  $ETD(\mathbf{X}, core(\mathbf{C})) > q_\alpha(D(\mathbf{C}, core(\mathbf{C})))$

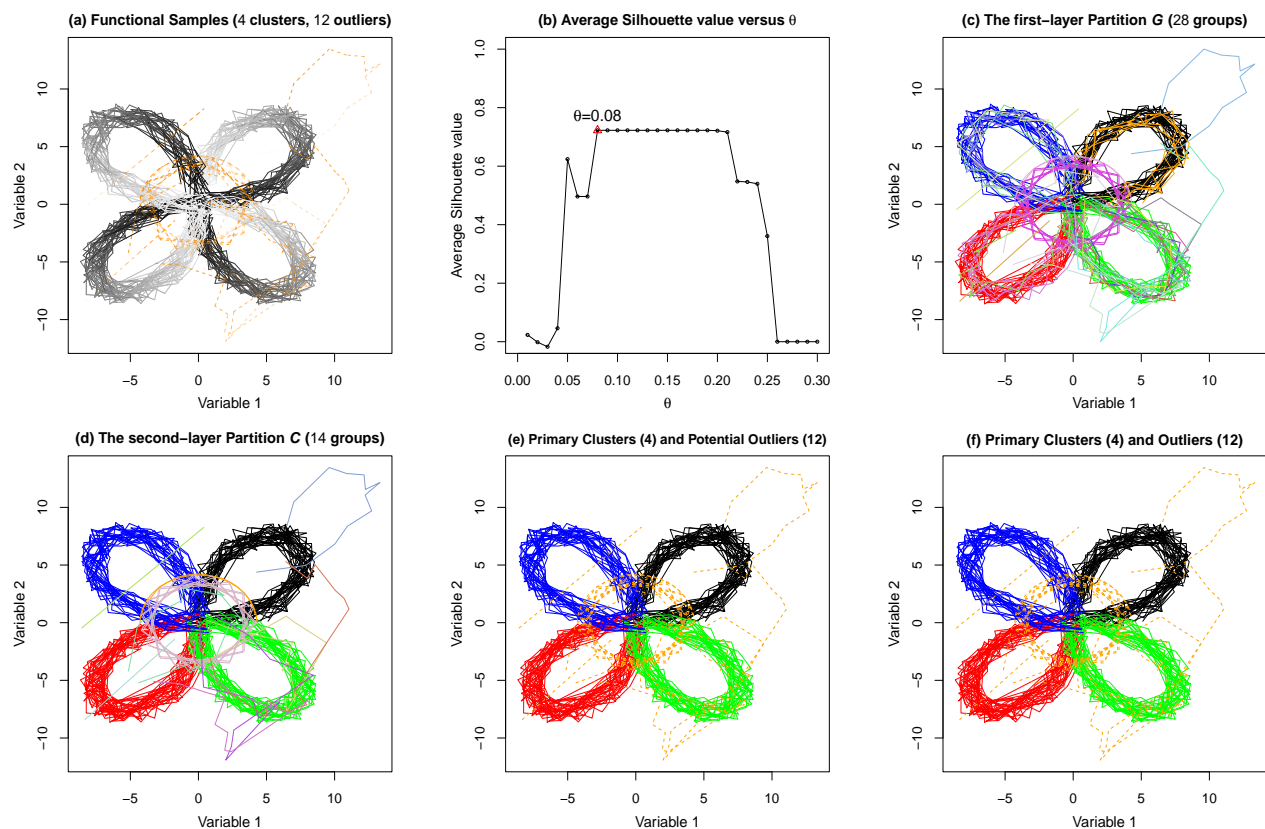


Figure 2: Example of stepwise clustering results. (a) Original clusters in black (transparency increases with time elapsed) mixed with outliers in orange, and (b) changes in the average silhouette value vs.  $\theta$ , (c) and (d) First- and second-layer partitions  $\mathbf{G}$  and  $\mathbf{C}$  from Algorithm 2, respectively, and (e) and (f) primary clusters  $\mathbf{C}_p$  and outliers  $O$  before and after applying the detection criterion, respectively, in Algorithm 3.

is the basic operation. The computational complexity of the worst cases in the above algorithms take  $\mathcal{O}(N^2)$ ,  $\mathcal{O}(N)$ , and  $\mathcal{O}(|\mathcal{C}_p| \times |O|)$ , respectively. Here,  $|\mathcal{C}_p| + |O| = I$ , and empirically,  $I \leq c\sqrt{N}$  for some  $c > 0$ . Therefore, most of the running time is spent on Algorithm 1, and this situation can be improved by parallel computation (Rossini et al. 2007).

### 3 Simulation Study

The aim of the simulation is to construct several scenarios, including the corruption of both outliers and time sparseness, and to demonstrate the robustness of our algorithm in comparison with existing methods. As to the assessment indexes, we adopt the adjusted Rand index (ARI, Hubert & Arabie 1985 Ferreira & Hitchcock 2009), percentage of correct outlier detection ( $p_c$ , i.e., the number of correctly detected outliers divided by the number of outliers), and percentage of false outlier detection ( $p_f$ , i.e., the number of falsely detected outliers divided by the number of nonoutliers) to assess the goodness of clustering and outlier detection. The settings with outliers and time sparseness are considered in Subsection 3.1, and the comparison results are given in Subsection 3.2. We examine our method RTLP, the ETD-based  $K$ -medoids and agglomerative hierarchical methods, and the model-based funHDDC (Schmutz et al. 2020). The optimal  $K$  was determined by the average silhouette value for the ETD-based methods and by the BIC for funHDDC.

#### 3.1 Simulation Settings

Here, we first list six types of scenarios, and describe the contamination and the time sparseness introduced in each scenario. The clustering scenarios we consider are as follows: amplitude variation, phase variation, horizontal shift, clover petals as closed curves, cyclone tracks mimicked by the curves starting from a similar location and diverting to various destinations, and helices with different radii.

For the sample  $\mathbf{f}_i$  ( $i = 1, \dots, N$ ) evaluated at the common time grid  $\mathbf{st} = \{\frac{k-1}{T-1}, k =$

$1, \dots, T\}$ , we have  $\mathbf{f}_i = \mathbf{m}_i + \mathbf{e}_i$ . For  $t \in \mathbf{st}$ ,  $\mathbf{m}(t) = (m^{(1)}(t), \dots, m^{(p)}(t))^\top$ , and  $\mathbf{e}_i(t) = (e^{(1)}(t), \dots, e^{(p)}(t))^\top$ . The measurement errors evaluated at the standard grid are denoted as  $\mathbf{e} = (\mathbf{e}^1, \mathbf{e}^2, \dots, \mathbf{e}^p)^\top$ , where  $\mathbf{e}^k = \{e^{(k)}(t), t \in \mathbf{st}\}$ . We assume that  $\mathbf{e}$  follows a normal distribution  $\mathcal{N}_{pT}(\mathbf{0}, C)$ , where  $C$  is a covariance matrix consisting of blocks  $C_{i,j} \in \mathbb{R}^{T \times T}$  for  $1 \leq i, j \leq p$ , and  $C_{i,j}(s, t)$  denotes the covariance between  $e^{(i)}(s)$  and  $e^{(j)}(t)$ . Assume that  $C_{i,j}(s, t)$  follows the Matérn cross-covariance ([Gneiting et al. 2010](#)) function as follows:

$$C_{ij}(s, t) = \begin{cases} \sigma_i^2 \mathcal{M}(|s - t|; \nu_i, \eta_i), & 1 \leq i = j \leq p, \\ \rho_{ij} \sigma_i \sigma_j \mathcal{M}(|s - t|; \nu_{ij}, \eta_{ij}), & 1 \leq i \neq j \leq p, \end{cases} \quad (2)$$

where  $\mathcal{M}(h; \nu, \eta) = \frac{2^{1-\nu}}{\Gamma(\nu)} (\eta h)^\nu \mathcal{K}_\nu(\eta h)$ ,  $h = |s - t| \in [0, 1]$ , and  $\mathcal{K}_\nu$  is a modified Bessel function of the second kind of order  $\nu$ . Here,  $\sigma^2$  is the marginal variance,  $\nu > 0$  adjusts smoothness, and  $\eta > 0$  is a scale parameter. Let  $\nu_{ij} = \frac{1}{2}(\nu_i + \nu_j)$ , and  $\nu_i$  is generated from the uniform distribution,  $\nu_i \sim \mathcal{U}(0.2, 0.3)$ . Let the matrix  $(\beta_{ij})_{i,j=1}^p$  be symmetric and nonnegative definite with diagonal elements  $\beta_{ii} = 1$  for  $i = 1, \dots, p$ , and nondiagonal elements  $\beta_{ij} \sim \mathcal{U}(0, 1)$  for  $1 \leq i < j \leq p$ , and  $\rho_{ij} = \beta_{ij} \frac{\Gamma(\nu_i + \frac{p}{2})^{1/2} \Gamma(\nu_j + \frac{p}{2})^{1/2}}{\Gamma(\nu_i)^{1/2} \Gamma(\nu_j)^{1/2}} \frac{\Gamma\{\frac{1}{2}(\nu_i + \nu_j)\}}{\Gamma\{\frac{1}{2}(\nu_i + \nu_j) + \frac{p}{2}\}}$  for  $1 \leq i \leq j \leq p$ .

Let the number of variables  $p = 3$ , and  $T$  be 50 equidistant points in  $[0, 1]$ ; the number of objects  $N = 150$ ; the number of clusters  $K = 3$ . Here,  $\sigma_1^2 = 0.05$ ,  $\sigma_2^2 = 0.2$ , and  $\sigma_3^2 = 0.3$ . Each cluster has an equal number of samples. For  $k = 1, \dots, K$  and  $v = 1, \dots, p$ , we have  $l \sim \mathcal{U}(1, p)$ , and  $r \sim \mathcal{B}(1/2)$ , where  $\mathcal{B}(b)$  represents a Bernoulli distribution with the probability  $b$ . All six clustering scenarios are described as follows:

Scenario 1 (amplitude variation):  $m^{(v)}(t) = 2v \cos\{(l + rv/4)\pi t\} + (-1)^r 3kv$ .

Scenario 2 (phase variation):  $m^{(v)}(t) = 2v \cos\{(l + rv/4)\pi h(t)\}$ . Let  $h(t) = \log_2(t + 1)$  when  $k = 1$ ,  $h(t) = t^2$  when  $k = 2, v = 1$ ,  $h(t) = 1 - \cos(\pi t/2)$  when  $k = 2, v = 2$ ,  $h(t) = \sin^2(\pi t/2)$  for  $k = 2, v = 3$ ,  $h(t) = t^3$  for  $k = 3, v = 1$ ,  $h(t) = \sin(\pi t/2)$  for  $k = 3, v = 2$ , and  $h(t) = t$  for  $k = 3, v = 3$ .

Scenario 3 (shift variation):  $m^{(v)}(t) = 6 \cos\{(l + v)\pi(t + 0.2lk)/2\}$ .

Scenario 4 (clover petals): Let  $m^{(1)}(t) = 5 \cos\{3w_k(t)\} \cos\{w_k(t)\}$ ,  $m^{(2)}(t) = 5 \cos\{3w_k(t)\} \sin\{w_k(t)\}$ ,

and  $m^{(3)}(t) = 5 \cos\{3w_k(t)\}$ , where  $w_k(t) = 1.01(t + k - 1) + 0.548$ .

Scenario 5 (cyclone tracks):

$$m^{(1)}(t) = \begin{cases} -5t - \sin(10\pi t), \\ 5 \sin(10\pi t), \\ 5t + \sin(10\pi t), \end{cases} \quad m^{(2)}(t) = \begin{cases} 11t^2, \\ 7t, \\ 5 \log_2(t + 1), \end{cases} \quad m^{(3)}(t) = \begin{cases} 7 \log_2(t + 1), & k = 1, \\ 14 \log_2(t + 1), & k = 2, \\ 21 \log_2(t + 1), & k = 3. \end{cases}$$

Scenario 6 (helixes with variable radii):

$$m^{(1)}(t) = \begin{cases} 5 \cos(10\pi t), \\ 5t \cos(20\pi t + 10), \\ 5t \sin(20\pi t + 10), \end{cases} \quad m^{(2)}(t) = \begin{cases} 5.5 \sin(10\pi t), \\ 5t \sin(20\pi t + 10), \\ 5 \log_2(t + 1), \end{cases} \quad m^{(3)}(t) = \begin{cases} 10t, & k = 1, \\ 10 - 10t, & k = 2, \\ 10t, & k = 3. \end{cases}$$

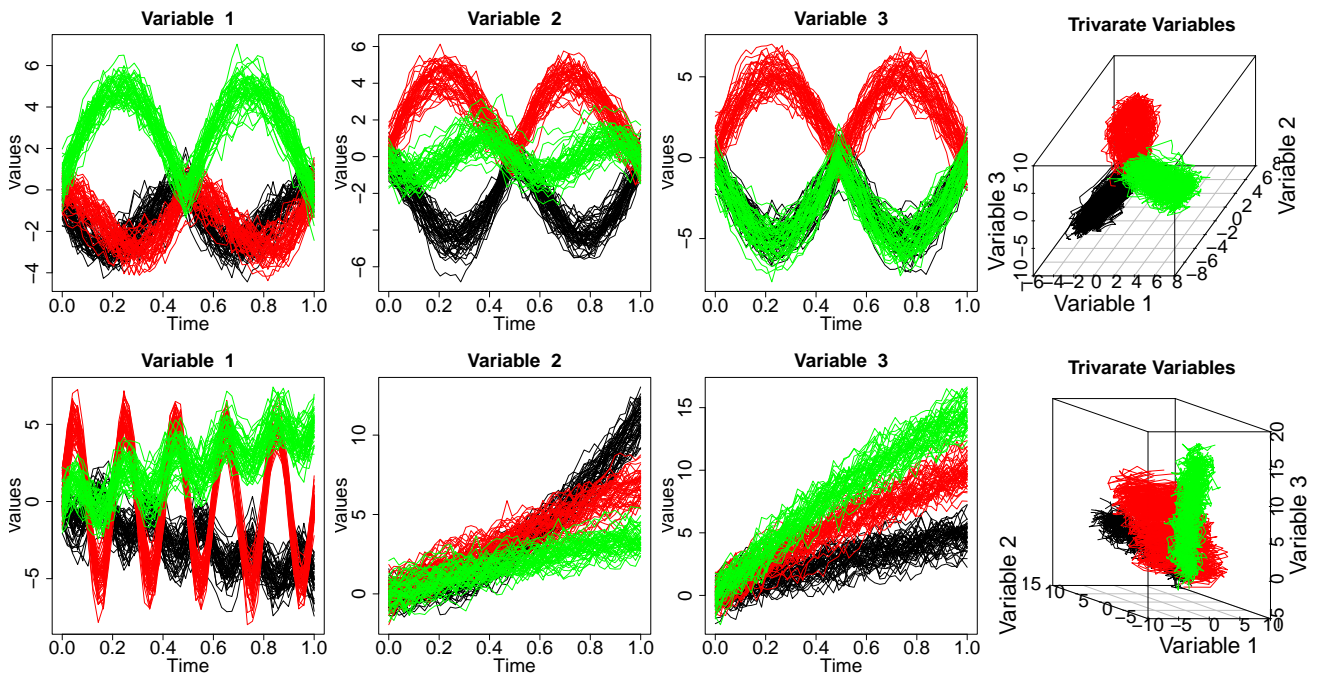


Figure 3: Top and bottom rows represent samples from Scenarios 4-5, respectively. Three clusters are represented in black, red, and green.

Scenarios 4 and 5 are representatives of the closed and nonclosed curves. We provide the visualization (Figure 3) and the clustering results of Scenarios 4 and 5 in this paper; the results for the remaining scenarios are provided in the Supplementary Material.

Next, we introduce three types of magnitude outliers (Contaminations 1-3), and three types of shape outliers (Contaminations 4-6), and introduce 10% outliers from these models to the aforementioned clustering scenarios. The visualization of Scenario 4 with various outlier settings is shown in Figure 4. The first and second rows in Figure 4 reveal the outliers showing abnor-



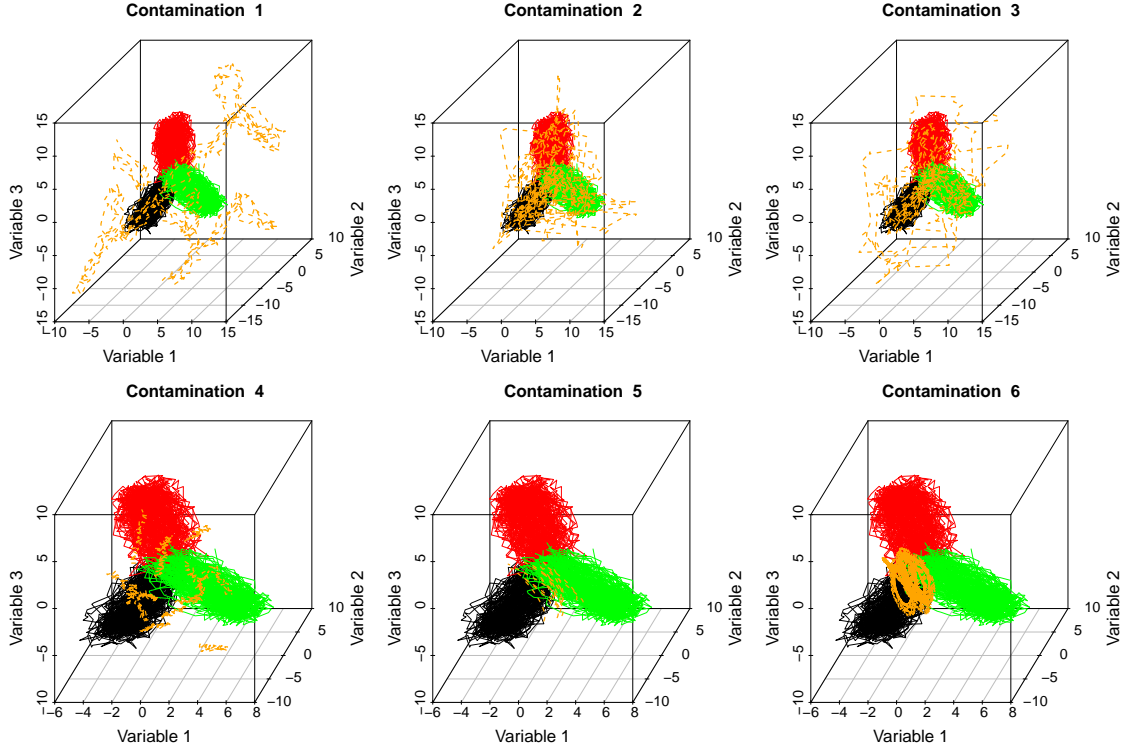


Figure 4: Visualization of Scenario 4 with a proportion 10% of outliers. Three clusters are labeled in solid black, red, and green, whereas the outliers are labeled in dashed orange.

malities in magnitude and shape, respectively.

Contamination 1 (pure outlier):  $\tilde{m}_i^{(v)}(t) = m_i^{(v)}(t) + rh$ . Here  $r$  is assigned to 1 if  $\mathcal{U}(-1, 1) > 0$ , otherwise  $r$  is  $-1$ , and  $h = \max\{|\min(m_i^{(v)}(t))|, |\max(m_i^{(v)}(t))|\}/2$ . Then,  $r$  and  $h$  below are generated in the same way as Contamination 1.

Contamination 2 (peak outlier):  $\tilde{m}_i^{(v)}(t) = \begin{cases} m_i^{(v)}(t) + rh, & t \in [st, st + 0.1], \\ m_i^{(v)}(t), & \text{otherwise,} \end{cases}$  where  $st \sim \mathcal{U}(0, 0.9)$ .

Contamination 3 (partial outlier):  $\tilde{m}_i^{(v)}(t) = \begin{cases} m_i^{(v)}(t) + rh, & t \in [st, 1], \\ m_i^{(v)}(t), & \text{otherwise,} \end{cases}$  where  $st \sim \mathcal{U}(0, 0.5)$ .

Contamination 4 (shape outlier I):  $c \sim \mathcal{U}(\min(m_i^{(v)}(t))/2, \max(m_i^{(v)}(t))/2)$ , and  $s \sim \mathcal{U}(-2v, 2v)$   $\tilde{m}_i^{(v)}(t) = c + st + \epsilon_i(t)$ , and  $\epsilon_i(t) \sim \mathcal{U}(-0.3, 0.3)$ .

Contamination 5 (shape outlier II):  $\tilde{m}_i^{(1)}(t) = s^{(1)}(t) + h \cos(0.5\pi t) + a$ ,  $\tilde{m}_i^{(2)}(t) = s^{(2)}(t) + h \sin(0.5\pi t) + a$ , and  $\tilde{m}_i^{(3)}(t) = s^{(3)}(t) - h \cos(0.5\pi t) + a$ , where  $s^{(v)}(t) = \min(m_i^{(v)}(t))/2 + \max(m_i^{(v)}(t))/2$  ( $v = 1, 2, 3$ ), and  $a \sim \mathcal{U}(-h, 0)$ . The  $s^{(v)}(t)$  below is generated in the same way.

Contamination 6 (shape outlier III):  $\tilde{m}_i^{(1)}(t) = s^{(1)}(t) + h \cos(30\pi t) + a$ ,  $\tilde{m}_i^{(2)}(t) = s^{(2)}(t) + h \sin(30\pi t) + a$ , and  $\tilde{m}_i^{(3)}(t) = s^{(3)}(t) - h \cos(30\pi t) + a$ , where  $a \sim \mathcal{U}(-h, 0)$ .

In addition, we introduce the parameters  $p_{size}$  and  $p_{curve}$  to ensure that each curve has unique time measurements in order to verify that our clustering algorithm can handle sparse multivariate functional data. Here,  $p_{size}$  represents the number of curves with missing values divided by the total number of the observed curves, and  $p_{curve}$  represents the number of missing points for curves with missing values divided by the cardinality of the standard time grid set. We conduct the simulation for  $p_{size} = 100\%$  and  $p_{curve}$  ranging from 0% up to 60%.

Figure 5 shows the visualization of Scenario 5 with 10% proportion of pure magnitude outliers for different time sparseness  $p_{curve} = 0\%$ , 30%, and 60% and  $p_{size} = 100\%$ , respectively. As data trajectories become sparser, the clustering patterns are harder to recognize, and the clustering is expected to be more challenging.

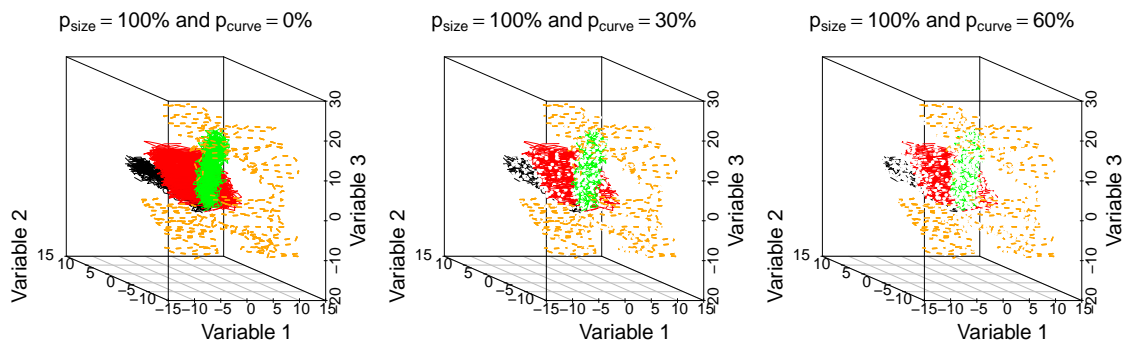


Figure 5: Visualization of Scenario 5 with 10% pure magnitude outliers for  $p_{curve} = 0\%$ , 30%, and 60% separately and  $p_{size} = 100\%$  in all above settings. The three clusters are shown in black, red, and green, and the outliers are indicated in orange.

### 3.2 Clustering Performance

We apply ARI,  $p_c$ , and  $p_f$  to assess the goodness of clustering and outlier detection. ARI can be applied when the actual clusters are known. It estimates the matching between the actual partition and the estimated partitions, and it is zero in the case of random partitions and one in the case of perfect agreement between two partitions.

To illustrate the robustness of our algorithm, we compare the ARI among ETD-based RTLP, agglomerative hierarchical clustering,  $K$ -medoids methods, and funHDDC. In particular, we apply these four methods to multivariate functional data and to each marginal functional data separately. The ARI for multivariables and the average ARI over marginal variables are obtained to evaluate the investigated method under the two situations. We denote the method applied to multivariate (univariate) functional data as its multivariate (univariate) version. Note that the difference between ETD-based multivariate clustering methods and univariate clustering ones only lies in the calculation of ETD (see step 1) in Section 2.4).

Figures 6 and 7 show the boxplots of  $ARI^2$  for Scenarios 4 and 5 under different outlier contaminations and missing time measurements. Overall, the ETD-based clustering methods perform better than funHDDC, and the multivariate RTLP exhibits the best performance in achieving the ARI with the highest mean and has a very low standard deviation in almost all cases. We view the results from horizontal and vertical perspectives.

From a horizontal perspective of Figures 6 and 7, there are three summaries under the same time measurement setting. First, the multivariate ETD-based methods perform better than their corresponding univariate methods in the clustering, as seen from the median of the boxplots. Second, the ETD-based clustering methods have better clustering precision than funHDDC, as seen from the differences among the boxplots in terms of the median and range. Finally, outlier contaminations may lead to a drop in the clustering precision depending on the outlier types. For example, Contaminations 5 and 6 in Scenario 4 influence the clustering precision of multivariate agglomerative hierarchical and  $K$ -medoids with funHDDC, whereas multivariate RTLP is rarely influenced.

From a vertical perspective of Figures 6 and 7, we observe two patterns. First, the clustering pattern influences the clustering precision of the ETD-based methods when there are missing values. The precision of clustering in Scenario 4 remains almost identical even when  $p_{curve}$  changes from 0% to 30% and then to 60%; the multivariate RTLP exhibits the best performance, followed

by multivariate agglomerative hierarchical and  $K$ -medoids. However, the clustering precision of multivariate RTLP in Scenario 5 decreases when  $p_{curve} = 60\%$ , whereas the precision of multivariate agglomerative hierarchical and  $K$ -medoids are not influenced much. From the pattern of Scenario 5 (Figure 5), we speculate that because of too much sparseness, the partition of the

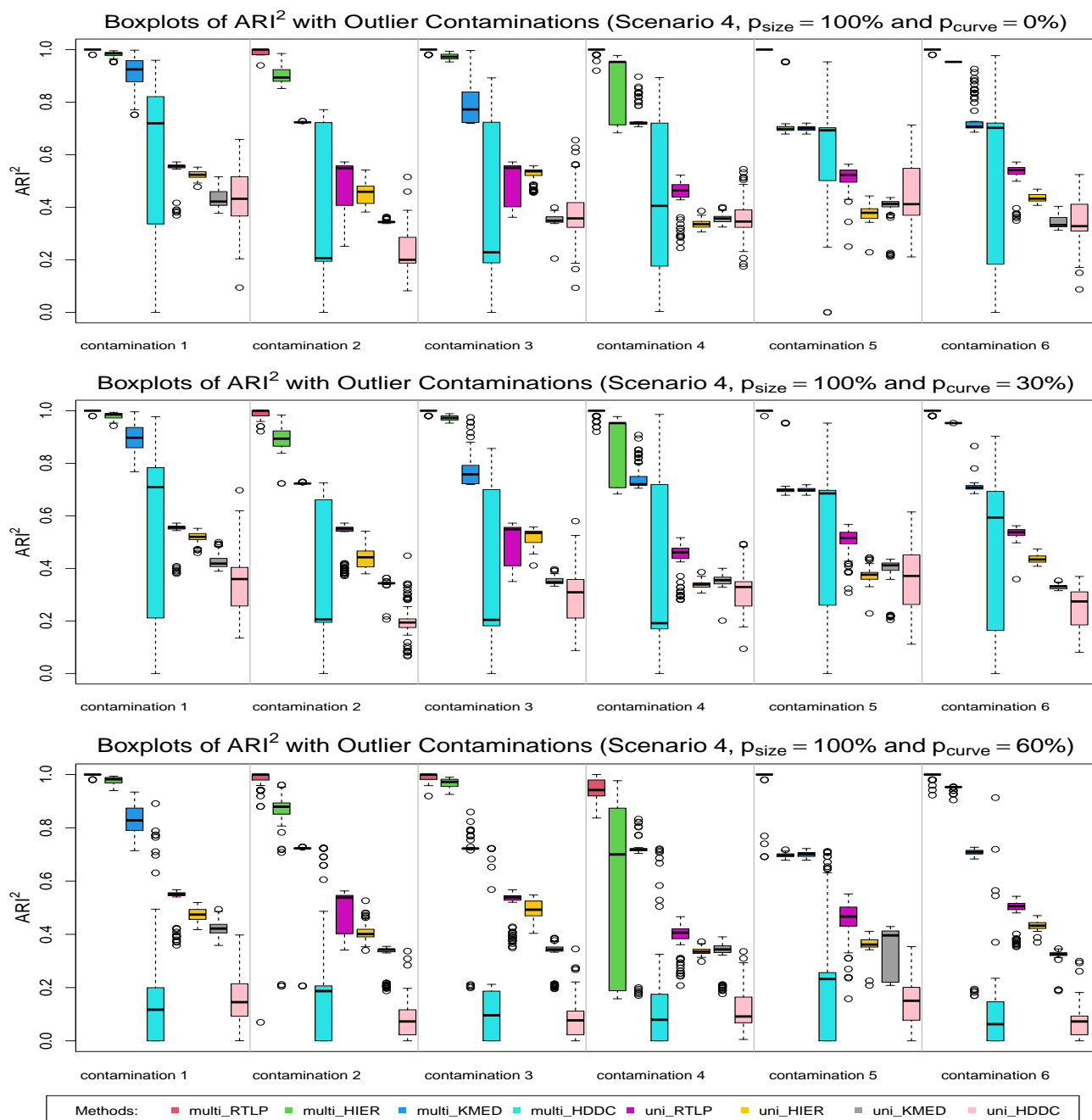


Figure 6: Panels from the top to bottom display the boxplots of  $ARI^2$  in Scenario 4 for  $p_{curve} = 0\%$ ,  $30\%$  and  $60\%$ . Eight methods are compared under all settings with six contaminations. Here,  $K = 3$ , and there are 100 simulation replicates. The methods, from left to right, are the multivariate and average marginal univariate versions of RTLP, agglomerative hierarchical,  $K$ -medoids, and funHDDC methods.

curves in the middle cluster and that of the curves at the edge of the remaining clusters are the same with multivariate RTLP. However, the multivariate agglomerative hierarchical clustering seeks to build a hierarchy of clusters from each observation as a separate cluster from all observations merged into one cluster, and the multivariate  $K$ -medoids searches the robust  $K$  sets of

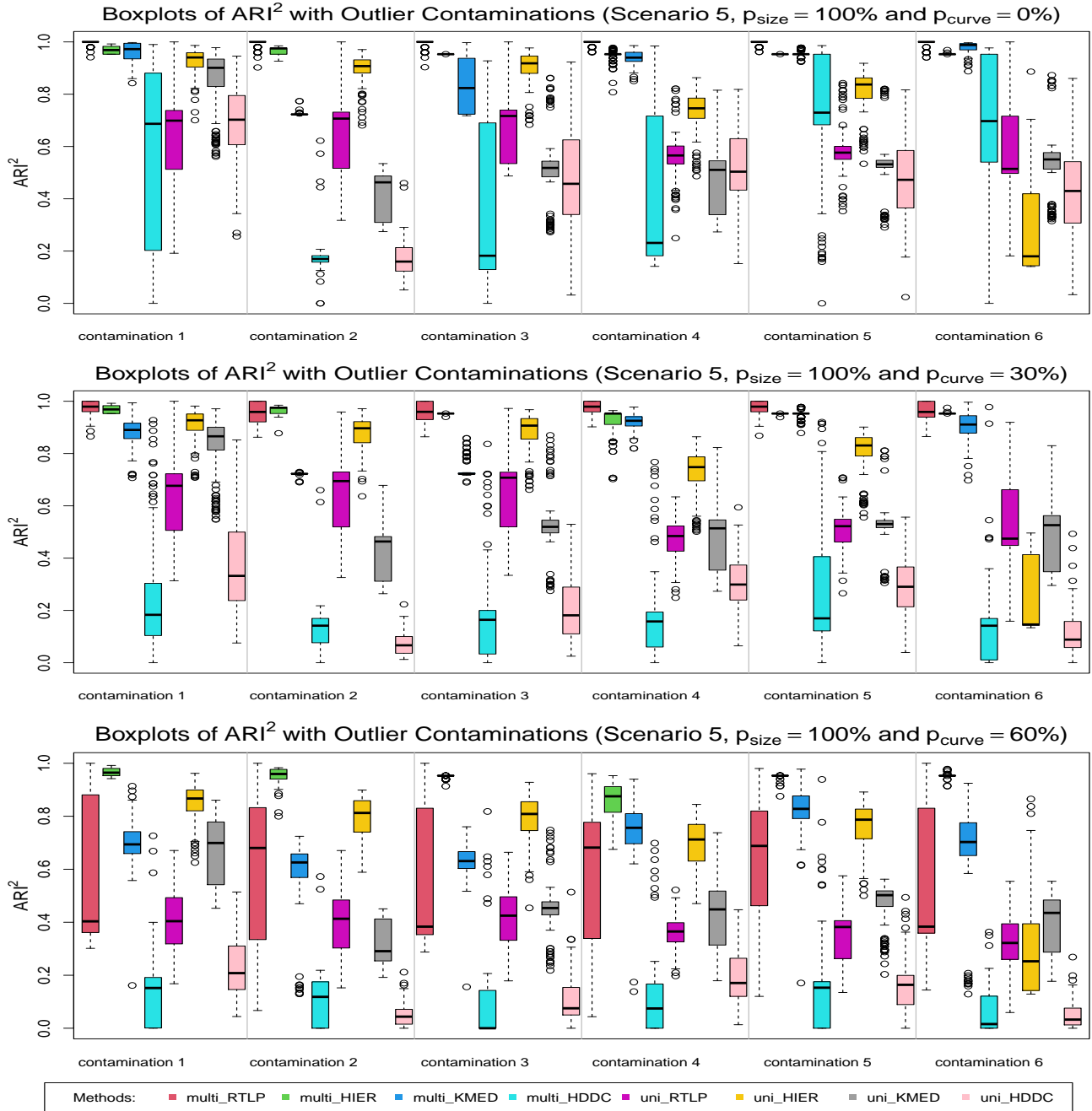


Figure 7: Panels from the top to bottom display the boxplots of  $ARI^2$  in Scenario 5 for  $p_{curve} = 0\%$ ,  $30\%$  and  $60\%$ . Eight methods are compared under all settings with six contaminations. Here,  $K = 3$ , and there are 100 simulation replicates. The methods, from left to right, are the multivariate and average marginal univariate versions of RTLP, agglomerative hierarchical,  $K$ -medoids, and funHDDC methods.

clusters and chooses one medoid as the center of the cluster. Second, multivariate and univariate funHDDC methods are not stable in clustering and are affected by the missing values, which can be seen from the movement of the boxplots vertically.

The multivariate RTLP usually behaves the best when the curve sparseness  $p_s$  is not greater than 50% – 60%. Although the results are not reported in this paper, the running time is stable for all ETD-based clustering methods but shows a significant standard deviation for funHDDC. Hence, we recommend multivariate RTLP when the data objects, i.e., multivariate functional data, are not too sparse, and we acknowledge that the agglomerative hierarchical clustering is a good alternative for very sparse cases.

### 3.3 Outlier Detection Performance

With regard to outlier detection,  $p_c$  and  $p_f$  are reported only for multivariate and marginal RTLP methods because of their capabilities of recognizing outliers. Specifically, we obtained  $p_c$  ( $p_f$ ) from the marginal RTLP for each variable and used the average  $p_c$  ( $p_f$ ) over different variables to represent the performance of univariate RTLP in the outlier detection.

Table 1 lists  $p_c$  and  $p_f$  in Scenarios 4 and 5 when  $p_{curve}$  increases from 0% to 30% and 60%. Usually, the multivariate RTLP exhibits high outlier detection accuracy as  $p_c$  increases close to 100% and a lower  $p_f$ , written in bold. The  $p_f$  reported in the multivariate RTLP is below 1% (7.1%) in the case of Contaminations 1-3 (4-6). Generally, the accuracy of the outlier detection when the scenario is mixed with shape outliers decreases with an increase of  $p_{curve}$ . It is seen from the decreasing  $p_c$  and increasing  $p_f$  in the case of Contaminations 4-6 when  $p_{curve}$  increases from 0% to 60%. Note that a tolerable decrease of 10% in  $p_c$  occurs in Scenario 4 (Contamination 4,  $p_{curve} = 60\%$ ), when the clustering precision of the multivariate RTLP exhibits a slight fluctuation (see Figure 6). In addition, there is a 40% decrease in  $p_c$  and a 7% increase in  $p_f$  in Scenario 5 mixed with Contaminations 4 and 5. In the meantime, the clustering precision of the multivariate RTLP also decreases (see Figure 7).

Table 1: Correct outlier detection percentage  $p_c$  (%) and false outlier detection percentage  $p_f$  (%) for multi\_RTLP and uni\_RTLP with different outlier contaminations for Scenarios 4 and 5. We indicate multi\_RTLP (uni\_RTLP) multivariate (univariate) in the RTLP version, and higher  $p_c$  and lower  $p_f$  values for each setting given the contamination and  $p_{curve}$  are indicated in bold. The proportion of outliers is 10%, and  $p_{size}$  is 100% for all settings. Simulations were conducted with 100 replicates.

(a) Scenario 4

RTLP version		Contamination 1		Contamination 2		Contamination 3	
		$p_c$	$p_f$	$p_c$	$p_f$	$p_c$	$p_f$
0%	multivariate	<b>99.8</b> (1.1)	<b>0.0</b> (0.0)	<b>97.6</b> (3.4)	<b>0.0</b> (0.1)	<b>99.2</b> (2.2)	<b>0.0</b> (0.0)
	univariate	98.2 (6.3)	0.9 (2.9)	92.7 (10.2)	4.1 (5.6)	93.0 (9.8)	3.6 (5.1)
30%	multivariate	<b>99.9</b> (0.7)	<b>0.0</b> (0.1)	<b>97.5</b> (4.0)	<b>0.0</b> (0.2)	<b>99.2</b> (2.2)	<b>0.0</b> (0.0)
	univariate	98.3 (5.7)	1.0 (3.0)	95.1 (8.1)	2.7 (4.7)	92.7 (9.9)	3.4 (5.0)
60%	multivariate	<b>100.0</b> (0.0)	<b>0.0</b> (0.1)	<b>95.8</b> (7.2)	<b>0.6</b> (3.6)	<b>98.3</b> (3.1)	<b>0.0</b> (0.2)
	univariate	97.5 (7.2)	1.4 (3.4)	90.9 (8.2)	2.8 (4.7)	92.2 (7.2)	2.1 (4.2)
RTLP version		Contamination 4		Contamination 5		Contamination 6	
		$p_c$	$p_f$	$p_c$	$p_f$	$p_c$	$p_f$
0%	multivariate	<b>98.6</b> (4.0)	<b>0.0</b> (0.0)	<b>100.0</b> (0.0)	<b>0.0</b> (0.0)	<b>99.7</b> (1.3)	<b>0.0</b> (0.0)
	univariate	62.2 (15.2)	1.8 (4.0)	86.0 (11.1)	1.3 (3.9)	92.2 (8.2)	1.1 (3.3)
30%	multivariate	<b>97.8</b> (5.0)	<b>0.0</b> (0.0)	<b>100.0</b> (0.0)	<b>0.0</b> (0.1)	<b>99.1</b> (2.3)	<b>0.0</b> (0.0)
	univariate	60.4 (13.0)	2.3 (4.1)	84.8 (11.1)	1.1 (3.5)	92.2 (5.3)	0.2 (1.2)
60%	multivariate	<b>81.5</b> (15.1)	<b>0.0</b> (0.2)	<b>95.7</b> (19.4)	<b>0.0</b> (0.1)	<b>99.0</b> (2.8)	<b>0.0</b> (0.2)
	univariate	39.4 (10.9)	1.1 (2.9)	67.5 (19.9)	2.2 (4.5)	80.8 (6.9)	1.8 (3.9)

(b) Scenario 5

RTLP version		Contamination 1		Contamination 2		Contamination 3	
		$p_c$	$p_f$	$p_c$	$p_f$	$p_c$	$p_f$
0%	multivariate	<b>100.0</b> (0.0)	<b>0.1</b> (0.3)	<b>98.6</b> (2.9)	<b>0.1</b> (0.3)	<b>99.7</b> (1.5)	<b>0.0</b> (0.1)
	univariate	99.9 (0.7)	0.8 (0.8)	98.0 (2.2)	0.5 (0.6)	98.7 (2.1)	0.4 (0.5)
30%	multivariate	<b>100.0</b> (0.6)	<b>0.7</b> (0.7)	95.1 (5.1)	<b>0.7</b> (0.7)	<b>99.6</b> (1.6)	<b>0.2</b> (0.4)
	univariate	99.2 (2.4)	1.1 (0.9)	<b>96.1</b> (2.8)	0.8 (1.1)	97.2 (2.5)	0.7 (0.5)
60%	multivariate	<b>100.0</b> (0.0)	<b>4.0</b> (3.3)	<b>87.6</b> (10.4)	4.9 (7.8)	<b>98.6</b> (2.7)	<b>2.8</b> (3.0)
	univariate	88.0 (5.7)	4.4 (1.8)	80.1 (6.2)	<b>3.7</b> (2.0)	85.9 (4.6)	3.4 (1.6)
RTLP version		Contamination 4		Contamination 5		Contamination 6	
		$p_c$	$p_f$	$p_c$	$p_f$	$p_c$	$p_f$
0%	multivariate	<b>99.8</b> (1.1)	<b>0.1</b> (0.3)	<b>100.0</b> (0.0)	<b>0.1</b> (0.3)	<b>99.9</b> (0.9)	<b>0.0</b> (0.1)
	univariate	42.2 (9.1)	1.3 (2.4)	49.7 (10.1)	1.1 (1.5)	97.7 (3.9)	1.4 (1.6)
30%	multivariate	<b>98.5</b> (5.4)	<b>0.8</b> (0.8)	<b>99.5</b> (4.3)	<b>1.0</b> (1.0)	<b>99.9</b> (0.8)	<b>0.2</b> (0.3)
	univariate	40.6 (9.8)	6.0 (3.3)	46.9 (5.1)	4.8 (3.2)	82.0 (7.0)	1.8 (1.5)
60%	multivariate	<b>57.5</b> (32.8)	7.1 (7.1)	<b>64.5</b> (41.5)	<b>6.8</b> (7.1)	<b>100.0</b> (0.6)	<b>3.1</b> (5.3)
	univariate	37.9 (9.2)	<b>6.8</b> (1.2)	47.2 (4.8)	7.3 (1.7)	66.4 (3.0)	7.9 (2.4)

Given the excellent performance in the outlier-resistant clustering of RTLP and the stable running time regardless of the corruption by outliers and the influence of irregular time grids, we highly recommend RTLP as an outlier-resistant clustering method for multivariate functional data when the average  $p_{curve}$  is not very high. Furthermore, RTLP can effectively block outliers in the primary clusters if there are concerns about outliers.

## 4 Application to Northwest Pacific Tropical Cyclone Tracks

A cyclone ([Society 2000](#)) is a large-scale air mass that rotates around an intense center of low-atmospheric-pressure center. The word “tropical” in the term “tropical cyclone” refers to the geographical origin of these systems, which form almost exclusively over tropical seas. The rising and cooling of the swirling air results in formation of clouds and precipitation. Although most cyclones have a life cycle of 3-7 days ([Australia 2008](#)), some systems can last for weeks if the environment is favorable. The global tropical cyclones tracks from version 4 of the International Best Track Archive for Climate Stewardship (IBTrACS v04, [Knapp et al. 2010](#)) are available [online](#). We extracted 4051 Northwest Pacific (see [Figure 8 \(a\)](#)) cyclone tracks between 1884 and 2021 for clustering analysis. The data are usually measured every three hours. We aligned the time of generation and disappearance to be 0 and 1, respectively, for each trajectory.

Using RTLP, we determine  $\theta = 0.22$  according to the maximum silhouette value when  $\theta$  changes from 0.01 to 0.3 in steps of 0.01 and with  $p_m = 0.05$  and  $\alpha = 0.85$ . We obtain two clusters according to the geographic trajectories of the cyclone centers; the first cluster has 3417 tracks, and the second one has 627 curves. The clustering pattern is consistent with the pattern reported by [Misumi et al. \(2019\)](#). Cyclones in the first cluster ([Figures 8 \(b\) and \(c\)](#)) mainly originate from the ocean to the east of the Philippines islands and sweep into inland Asia. Usually, they end in either eastern or southwestern China, blocked by a high-pressure system from the Chinese mainland. Cyclones in the second cluster ([Figures 8 \(d\) and \(e\)](#)) barely pass by mainland Asia, move toward North America, and disappear somewhere in the North Pacific. Seven curves that cannot be recognized in any cluster remain as outliers. They mainly show abnormal patterns or originate from a location far from the Philippines.

[Figure 8](#) also maps the geological tracks and their storm speed information per cluster. In the storm speed polar plot, the storm direction is taken as the angle and the storm speed norm as the radius. The storm moves in the direction pointed by the vector, in degrees east of north from 0 to 360 degrees. In addition, we use different colors to denote the number of neighbours



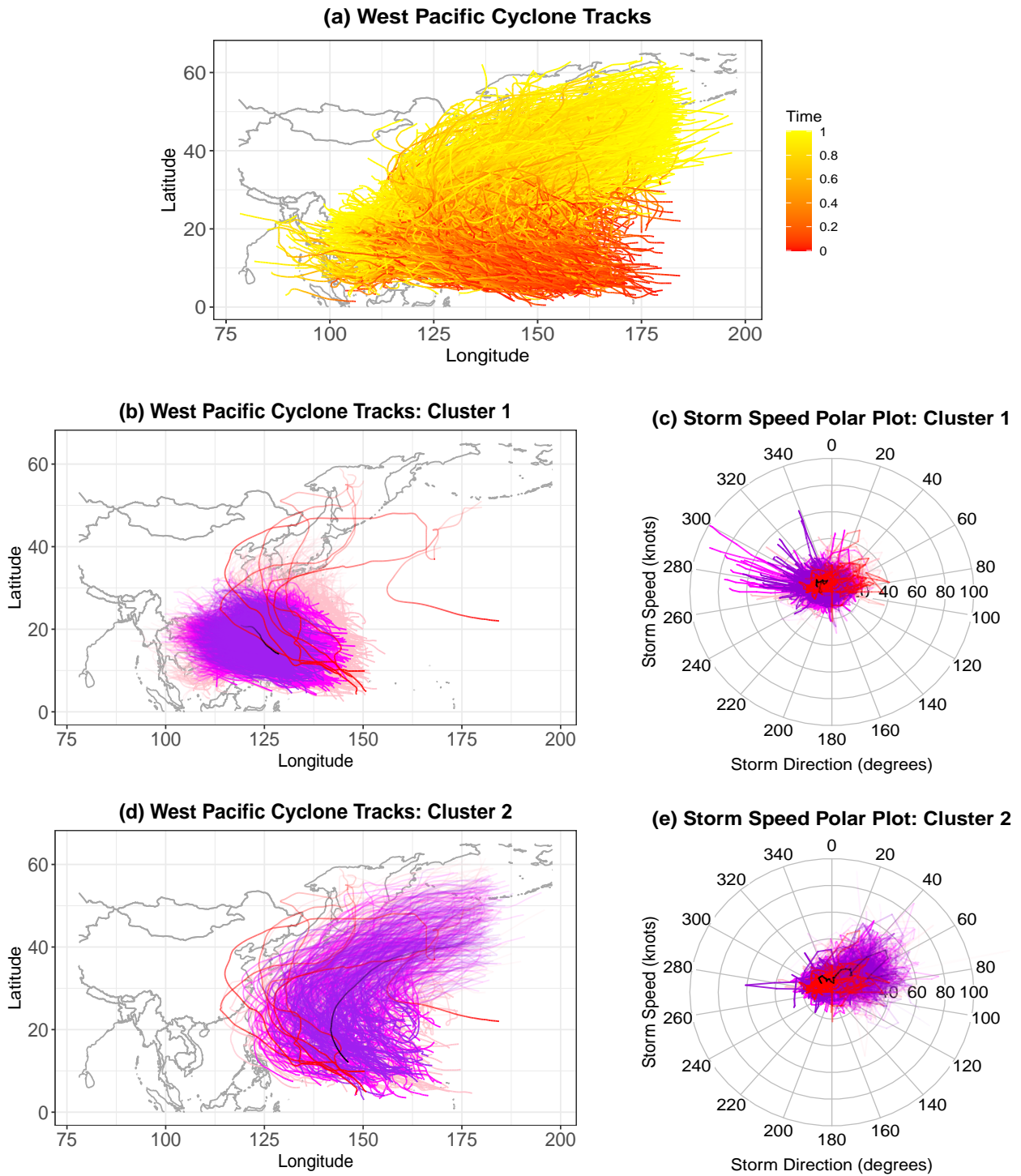


Figure 8: (a) 4051 Northwest Pacific cyclone tracks from 1884 to 2021. Each curve represents a full cyclone process, and the color changes gradually from red to yellow with time. (b) and (d) Cyclone trajectories obtained using our version of the trajectory boxplot (Yao et al. 2020). (c) and (e) Wind speed polar plot, with wind speed as the radius and wind speed direction as the angle. The black and red represent the median and outliers, respectively, and purple, magenta, and pink indicate the first, second, and third quartile curves, respectively.

inside a cluster, with black for the median, and purple, magenta, and pink to indicate the first, second, and third quartile regions, respectively, and red to indicate outliers.

The medians show the typical tracks in a cluster. The median in the first cluster (see Figure 8 (b)) is directed towards the northwest (direction between 270 and 360 degrees) with a storm speed of almost 10 knots, which is common for most cyclones in the first cluster. Usually, the wind speeds (i.e., the radius of the polar plot) of cyclones traveling inland decreases slowly because of reduction in the power of the cyclones. However, the median in the second cluster (see Figure 8 (d)) first shifts northwest and then turns eastwards (direction between 0 and 180 degrees), with the storm speed (i.e., the radius of the polar plot) increasing after the cyclones steer eastward. The cyclones in the second cluster that do not move inland but move to the North Pacific are influenced by the northward shift of high pressure over the Pacific (Times 2022).

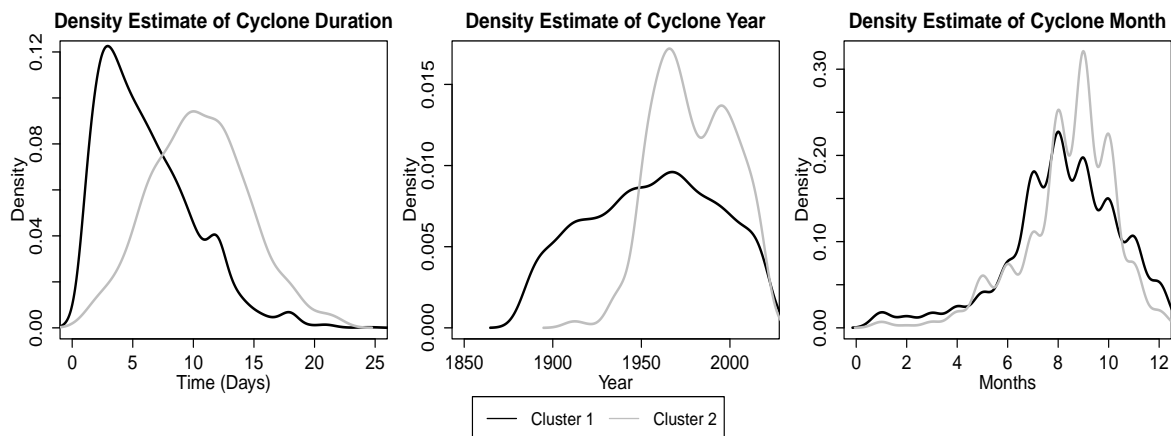


Figure 9: Extra time information from clusters 1 and 2 in the Northwest Pacific cyclones. The panels display the nonparametric density estimates of the lasting days, occurrence year, and occurrence month. The first cluster is labeled in black, and the second is in grey.

Besides geological and storm speed data, we use the lasting days and time of occurrence (Figure 9) of the cyclones to analyze the difference between the clusters. The first group of cyclones mostly lasts less than ten days, and the second group mainly lasts between five and fifteen days. On average, cyclones from the first cluster (Figure 8 (b)) travel a shorter distance than those from the second cluster (Figure 8 (d)). We see that the frequency of cyclones in both groups increased starting from the latter half of the 1940s to around 1960 (AOKI 1985), especially that of the cyclones that passed by Japan and Korea and reached the Sea of Okhotsk.

A remarkable decreasing trend in the cyclone frequency is noted between the late 1960s to around 1980. Subsequently, the cyclone frequency remained constant since the 1980s. Figure 9 shows that cyclones belonging to the second cluster mainly occurred after the 1950s; however, the ratio of the frequency of cyclones traveling to mainland Asia and directed to the North Pacific is around two versus one after 1950. High pressure (Times 2022) in the Sea of Okhotsk in eastern Russia and low pressure to the east of the Philippines have induced shifts in the direction of cyclones since the 1950s. Cyclones in the first cluster mainly occur from July to November, whereas those in the second cluster are concentrated between August and October. The increasing frequency of the cyclones is assumed to be related to global warming (Van Aalst 2006), which has also influenced the rise of seawater levels and surging tides smacked in low-lying areas.

## 5 Discussion

We defined an ETD measure and proposed a novel outlier-resistant two-layer partition (i.e., RTLP) clustering method. We proved that the ETD is a semimetric that can be applied to multivariate functional data with either fixed or irregularly spaced, imbalanced time grids. In addition, we separated our RTLP method into two-layer partition clustering and cluster and outlier recognition algorithms.

First, the two-layer partition clustering algorithm groups curves into disjoint sets by defining neighbours and the core and then merges these groups into a set of disjoint clusters. Next, the cluster and outlier recognition algorithm determines the final primary clusters and outliers. The time complexity of the whole algorithm majorly lies in the calculation of the distance across curves, which requires  $\mathcal{O}(N^2)$  time; the time complexity can be reduced through parallel computation. Regarding parameter selection, we choose the optimal  $\theta$  as the parameter with the highest revised average silhouette value and recommend  $p_m \leq 0.05$  and  $0.85 \leq \alpha \leq 0.9$ .

The existing distance-based methods, such as the classical  $K$ -medoids and agglomerative hierarchical clustering, can be naturally combined with ETD. Using simulations, we compared the clustering results of the ETD-based RTLP, agglomerative hierarchical methods,  $K$ -medoids,

and the model-based funHDDC. The RTLP method exhibited excellent performance in terms of both clustering curves and outlier detection; the performance decreased in the following order: the RTLP method, ETD-based agglomerative hierarchical clustering and  $K$ -medoid clustering, and finally, the funHDDC algorithm. The running time of ETD-based methods was stable for a fixed sample size, and it decreased as the time grid became sparser. Overall, RTLP has a significant advantage in terms of clustering precision regardless of the outliers and the time sparseness settings.

In future works, the RTLP and current clustering methods can be applied to more general sparse (multivariate) functional data, where the measurement can be observed for some variables but could be missing for other variables for one index (more types of sparseness are described in [Qu & Genton 2022](#)), which requires a more general distance measure. In addition, the aforementioned clustering methods can be applied to multivariate nonfunctional data. The bridge between our clustering method and multivariate nonfunctional data can be the  $L^p$  distance ([Bourbaki 2013](#)) for  $p = 1$ ,  $p = 2$ , and  $p = \infty$ . Another research direction is to cluster images or surfaces ([Chen et al. 2005](#), [Genton et al. 2014](#)); this would require defining the distance between the images.

## Appendix

The three algorithms in the RTLP clustering method are provided here. Algorithm 1 calculates the ETD between observations in  $S$ . Algorithm 2 merges curves into disjoint clusters, and Algorithm 3 determines a set of primary clusters  $C_p$  and  $O$ .

## References

- Abraham, C., Cornillon, P.-A., Matzner-Løber, E., & Molinari, N. (2003). Unsupervised curve clustering using B-splines. *Scandinavian Journal of Statistics*, 30(3), 581–595.
- Adams, R. A. & Fournier, J. J. (2003). *Sobolev Spaces*. Elsevier.
- Akaike, H. (1974). A new look at the statistical model identification. *IEEE Transactions on Automatic Control*, 19(6), 716–723.

---

**Algorithm 1** Elastic Time Distance Algorithm

---

1: **Input:**  $S = \{\mathbf{Y}_1, \dots, \mathbf{Y}_N\}$ ,  $\mathbf{t}_1, \dots, \mathbf{t}_N$   
2: **Initialize:** Zero matrix  $D \in \mathbb{R}^{N \times N}$ ,  $T = \max_{n=1}^N T_n$ ,  $\tilde{\mathbf{Y}}_n \leftarrow \text{Definition 3 } \forall n = 1, \dots, N$   
3: **function**  $ETD(\mathbf{Y}_i, \mathbf{Y}_j)$   
4:     **return**  $\max_{k=1}^T \sum_{d=1}^p (\tilde{Y}_{i,k}^{(d)} - \tilde{Y}_{j,k}^{(d)})^2$   
5: **for**  $i = 1$  to  $N - 1$  **do**  
6:     **for**  $j = i + 1$  to  $N$  **do**  
7:          $D_{i,j} \leftarrow ETD(\mathbf{Y}_i, \mathbf{Y}_j)$   
8:          $D_{j,i} \leftarrow D_{i,j}$   
9: **Output:**  $D$

---

---

**Algorithm 2** Two-Layer Partition Clustering Algorithm

---

1: **Input:**  $S = \{\mathbf{Y}_1, \dots, \mathbf{Y}_N\}$ ,  $D \in \mathbb{R}^{N \times N}$  from Algorithm 1,  $\theta \in [0.01, 0.2]$   
2: **Initialize:**  $\mathbf{G} \leftarrow \emptyset$ ,  $\mathbf{C} \leftarrow \emptyset$ ,  $M \leftarrow 0$ ,  $\tilde{S}_1 \leftarrow S$   
3: **while**  $\tilde{S}_{M+1} \neq \emptyset$  **do**  
4:      $M \leftarrow M + 1$   
5:      $\mathbf{G}^M \leftarrow nbr(\text{core}(\tilde{S}_M), \tilde{S}_M)$   
6:      $\tilde{S}_{M+1} \leftarrow \tilde{S}_M \setminus \mathbf{G}^M$   
7: **Initialize:**  $I \leftarrow 0$ ,  $\tilde{\mathbf{G}}_1 \leftarrow \mathbf{G}$   
8: **while**  $\tilde{\mathbf{G}}_{I+1} \neq \emptyset$  **do**  
9:      $I \leftarrow I + 1$   
10:      $\mathbf{C}^I \leftarrow \tilde{\mathbf{G}}_I^1$   
11:      $nbrS \leftarrow \bigcup_{\mathbf{Y} \in \mathbf{C}^I} nbr(\mathbf{Y}, S)$   
12:     **for**  $A$  in  $\tilde{\mathbf{G}}_I \setminus \tilde{\mathbf{G}}_I^1$  **do**  
13:         **if**  $A \neq \emptyset$  and  $\text{core}(A) \in nbrS$  **then**  
14:              $\mathbf{C}^I \leftarrow \mathbf{C}^I \cup A$   
15:      $\tilde{\mathbf{G}}_{I+1} \leftarrow \tilde{\mathbf{G}}_I \setminus \mathbf{C}^I$   
16: **Output:**  $\mathbf{C}$

---

Al Abid, F. B. (2014). A novel approach for PAM clustering method. *International Journal of Computer Applications*, 86(17), 1–5.

Antoniadis, A., Brossat, X., Cugliari, J., & Poggi, J.-M. (2013). Clustering functional data using wavelets. *International Journal of Wavelets, Multiresolution and Information Processing*, 11(01), 1350003.

AOKI, T. (1985). A climatological study of typhoon formation and typhoon visit to Japan. *Meteorology and Geophysics*, 36, 61–118.

Australia, S. S. (2008). Tropical cyclones. <https://www.ausstormscience.com/tropical-cyclones/>. accessed: 27.08.2021.

---

**Algorithm 3** Cluster and Outlier Recognition Algorithm

---

```
1: Input:  $S = \{\mathbf{Y}_1, \dots, \mathbf{Y}_N\}$ ,  $D$  from Algorithm 1,  $\mathbf{C}$  from Algorithm 2,  $p_m, \alpha$ 
2: Initialize:  $\mathbf{C}_p \leftarrow \emptyset$ ,  $O_p \leftarrow \emptyset$ ,  $O \leftarrow \emptyset$ ,  $B \leftarrow 0$ 
3: for  $i$  in  $1, \dots, |\mathbf{C}|$  do
4:   if  $|C_i| > Np_m$  then
5:      $B \leftarrow B + 1$ 
6:      $\mathbf{C}_p^B \leftarrow C_i$ 
7:   else
8:      $O_p \leftarrow O_p \cup C_i$ 
9:   if  $|O_p| > 0$  and  $|\mathbf{C}_p| > 0$  then
10:    for  $\mathbf{X}$  in  $O_p$  do
11:      if  $ETD(\mathbf{X}, core(C)) > q_\alpha(D(C, core(C))) \forall C \in \mathbf{C}_p$  then
12:         $O \leftarrow O \cup \mathbf{X}$ 
13:      else
14:         $\mathbf{C}_p^l \leftarrow \arg \min_{C \in \mathbf{C}_p} d_{ETD(\mathbf{X}, core(C))}(D(C, core(C)))$ 
15:         $\mathbf{C}_p^l \leftarrow \mathbf{C}_p^l \cup \mathbf{X}$ 
16: Output:  $\mathbf{C}_p$  and  $O$ 
```

---

Batool, F. & Hennig, C. (2021). Clustering with the average silhouette width. *Computational Statistics & Data Analysis*, 158, 107190.

Biernacki, C., Celeux, G., & Govaert, G. (2000). Assessing a mixture model for clustering with the integrated completed likelihood. *IEEE Transactions on Pattern Analysis and Machine Intelligence*, 22(7), 719–725.

Boullé, M. (2012). Functional data clustering via piecewise constant nonparametric density estimation. *Pattern Recognition*, 45(12), 4389–4401.

Bourbaki, N. (2013). *Topological Vector Spaces: Chapters 1–5*. Springer Science & Business Media.

Bouveyron, C. & Jacques, J. (2011). Model-based clustering of time series in group-specific functional subspaces. *Advances in Data Analysis and Classification*, 5(4), 281–300.

Centofanti, F., Lepore, A., & Palumbo, B. (2021). Sparse and smooth functional data clustering. *arXiv preprint arXiv:2103.15224*.

Chen, Y., Liu, X., Li, X., Liu, X., Yao, Y., Hu, G., Xu, X., & Pei, F. (2017). Delineating urban functional areas with building-level social media data: A dynamic time warping (DTW) distance based K-medoids method. *Landscape and Urban Planning*, 160, 48–60.

Chen, Y., Wang, J. Z., & Krovetz, R. (2005). Clue: Cluster-based retrieval of images by unsupervised learning. *IEEE Transactions on Image Processing*, 14(8), 1187–1201.

- Chiou, J.-M. & Li, P.-L. (2007). Functional clustering and identifying substructures of longitudinal data. *Journal of the Royal Statistical Society: Series B (Statistical Methodology)*, 69(4), 679–699.
- Choudhary, B. (1993). *The Elements of Complex Analysis*. New Age International.
- Collatz, L. (1966). *Functional Analysis and Numerical Mathematics*. New York, San Francisco, London: Academic Press.
- Cuesta-Albertos, J. A. & Fraiman, R. (2007). Impartial trimmed K-means for functional data. *Computational Statistics & Data Analysis*, 51(10), 4864–4877.
- Ferraty, F. & Vieu, P. (2006). *Nonparametric Functional Data Analysis: Theory and Practice*. Springer Science & Business Media.
- Ferreira, L. & Hitchcock, D. B. (2009). A comparison of hierarchical methods for clustering functional data. *Communications in Statistics-Simulation and Computation*, 38(9), 1925–1949.
- Floriello, D. & Vitelli, V. (2017). Sparse clustering of functional data. *Journal of Multivariate Analysis*, 154, 1–18.
- Gagolewski, M., Bartoszek, M., & Cena, A. (2016). Genie: A new, fast, and outlier-resistant hierarchical clustering algorithm. *Information Sciences*, 363, 8–23.
- García, M. L. L., García-Ródenas, R., & Gómez, A. G. (2015). K-means algorithms for functional data. *Neurocomputing*, 151, 231–245.
- Genton, M. G., Johnson, C., Potter, K., Stenchikov, G., & Sun, Y. (2014). Surface boxplots. *Stat*, 3(1), 1–11.
- Giacofci, M., Lambert-Lacroix, S., Marot, G., & Picard, F. (2013). Wavelet-based clustering for mixed-effects functional models in high dimension. *Biometrics*, 69(1), 31–40.
- Gneiting, T., Kleiber, W., & Schlather, M. (2010). Matérn cross-covariance functions for multivariate random fields. *Journal of the American Statistical Association*, 105(491), 1167–1177.
- Hartigan, J. A. & Wong, M. A. (1979). Algorithm AS 136: A K-means clustering algorithm. *Journal of the Royal Statistical Society. Series C (Applied Statistics)*, 28(1), 100–108.
- Horn, R. A. & Johnson, C. R. (1990). Norms for vectors and matrices. *In: Matrix Analysis*, (pp. 313–386).
- Horváth, L. & Kokoszka, P. (2012). *Inference for Functional Data with Applications*, volume 200. Springer Science & Business Media.

- Hsing, T. & Eubank, R. (2015). *Theoretical Foundations of Functional Data Analysis, with an Introduction to Linear Operators*, volume 997. John Wiley & Sons.
- Hubert, L. & Arabie, P. (1985). Comparing partitions. *Journal of Classification*, 2(1), 193–218.
- Ieva, F., Paganoni, A. M., Pigoli, D., & Vitelli, V. (2011). Multivariate functional clustering for the analysis of ECG curves morphology. In *Cladag 2011 (8th International Meeting of the Classification and Data Analysis Group)* (pp. 1–4).
- Ieva, F., Paganoni, A. M., Pigoli, D., & Vitelli, V. (2013). Multivariate functional clustering for the morphological analysis of electrocardiograph curves. *Journal of the Royal Statistical Society: Series C (Applied Statistics)*, 62(3), 401–418.
- Jacques, J. & Preda, C. (2013). Funclust: A curves clustering method using functional random variables density approximation. *Neurocomputing*, 112, 164–171.
- Jacques, J. & Preda, C. (2014a). Functional data clustering: A survey. *Advances in Data Analysis and Classification*, 8(3), 231–255.
- Jacques, J. & Preda, C. (2014b). Model-based clustering for multivariate functional data. *Computational Statistics & Data Analysis*, 71, 92–106.
- James, G. M. & Sugar, C. A. (2003). Clustering for sparsely sampled functional data. *Journal of the American Statistical Association*, 98(462), 397–408.
- Jeong, M.-H., Cai, Y., Sullivan, C. J., & Wang, S. (2016). Data depth based clustering analysis. In *Proceedings of the 24th ACM SIGSPATIAL International Conference on Advances in Geographic Information Systems* (pp. 1–10).
- Jung, Y., Park, H., Du, D.-Z., & Drake, B. L. (2003). A decision criterion for the optimal number of clusters in hierarchical clustering. *Journal of Global Optimization*, 25(1), 91–111.
- Kaufman, L. & Rousseeuw, P. J. (1990). Partitioning around medoids (program pam). *Finding Groups in Data: An Introduction to Cluster Analysis*, 344, 68–125.
- Knapp, K. R., Kruk, M. C., Levinson, D. H., Diamond, H. J., & Neumann, C. J. (2010). The international best track archive for climate stewardship (ibtracs) unifying tropical cyclone data. *Bulletin of the American Meteorological Society*, 91(3), 363–376.
- Kneip, A., Li, X., MacGibbon, K., & Ramsay, J. (2000). Curve registration by local regression. *Canadian Journal of Statistics*, 28(1), 19–29.
- Kodinariya, T. M. & Makwana, P. R. (2013). Review on determining number of cluster in K-means clustering. *International Journal*, 1(6), 90–95.



- Liu, X., Zhu, X.-H., Qiu, P., & Chen, W. (2012). A correlation-matrix-based hierarchical clustering method for functional connectivity analysis. *Journal of Neuroscience Methods*, 211(1), 94–102.
- Meng, Y., Liang, J., Cao, F., & He, Y. (2018). A new distance with derivative information for functional K-means clustering algorithm. *Information Sciences*, 463, 166–185.
- Misumi, T., Matsui, H., & Konishi, S. (2019). Multivariate functional clustering and its application to typhoon data. *Behaviormetrika*, 46(1), 163–175.
- Nielsen, F. (2016). Hierarchical clustering. In *Introduction to HPC with MPI for Data Science* (pp. 195–211). Springer.
- Olson, C. F. (1995). Parallel algorithms for hierarchical clustering. *Parallel Computing*, 21(8), 1313–1325.
- Park, J. & Ahn, J. (2017). Clustering multivariate functional data with phase variation. *Biometrics*, 73(1), 324–333.
- Peng, J. & Müller, H.-G. (2008). Distance-based clustering of sparsely observed stochastic processes, with applications to online auctions. *The Annals of Applied Statistics*, 2(3), 1056–1077.
- Qu, Z. & Genton, M. G. (2022). Sparse functional boxplots for multivariate curves. *Journal of Computational and Graphical Statistics*, to appear.
- Ramsay, J. O. & Silverman, B. W. (2005). *Functional Data Analysis*. Springer Series in Statistics.
- Ronchetti, E. (2021). The main contributions of robust statistics to statistical science and a new challenge. *Special Issue on the Centenary of Metron. Metron: International Journal of Statistics*, 79(2), 127–135.
- Rossini, A. J., Tierney, L., & Li, N. (2007). Simple parallel statistical computing in R. *Journal of Computational and Graphical Statistics*, 16(2), 399–420.
- Rousseeuw, P. J. (1987). Silhouettes: a graphical aid to the interpretation and validation of cluster analysis. *Journal of Computational and Applied Mathematics*, 20, 53–65.
- Samé, A., Chamroukhi, F., Govaert, G., & Aknin, P. (2011). Model-based clustering and segmentation of time series with changes in regime. *Advances in Data Analysis and Classification*, 5(4), 301–321.
- Sangalli, L. M., Secchi, P., Vantini, S., & Vitelli, V. (2010). K-mean alignment for curve clustering. *Computational Statistics & Data Analysis*, 54(5), 1219–1233.
- Schmutz, A., Jacques, J., Bouveyron, C., Cheze, L., & Martin, P. (2020). Clustering multivariate functional data in group-specific functional subspaces. *Computational Statistics*, 35, 1101–1131.

- Schwarz, G. (1978). Estimating the dimension of a model. *The Annals of Statistics*, 6(2), 461–464.
- Sheehy, A., Gasser, T., Molinari, L., & Largo, R. H. (2000). Contribution of growth phases to adult size. *Annals of Human Biology*, 27(3), 281–298.
- Shi, C., Wei, B., Wei, S., Wang, W., Liu, H., & Liu, J. (2021). A quantitative discriminant method of elbow point for the optimal number of clusters in clustering algorithm. *EURASIP Journal on Wireless Communications and Networking*, 2021(1), 1–16.
- Society, A. M. (2000). Glossary of meteorology: Cyclonic circulation. [https://glossary.ametsoc.org/wiki/Cyclonic\\_circulation](https://glossary.ametsoc.org/wiki/Cyclonic_circulation). accessed: 27.08.2021.
- Struyf, A., Hubert, M., & Rousseeuw, P. (1997). Clustering in an object-oriented environment. *Journal of Statistical Software*, 1(4), 1–30.
- Tabak, J. (2014). *Geometry: The Language of Space and Form*. Facts on File Math Library, Infobase Publishing.
- Tarpey, T. & Kinateder, K. K. (2003). Clustering functional data. *Journal of Classification*, 20(1), 093–114.
- Tibshirani, R., Walther, G., & Hastie, T. (2001). Estimating the number of clusters in a data set via the gap statistic. *Journal of the Royal Statistical Society: Series B*, 63(2), 411–423.
- Times, N. Y. (2022). Nature, science, animals - land, weather, volcanoes and earthquakes. <https://factsanddetails.com/japan/cat26/sub160/item856.html>. accessed: 03.01.2022.
- Van Aalst, M. K. (2006). The impacts of climate change on the risk of natural disasters. *Disasters*, 30(1), 5–18.
- Wang, J. & Su, X. (2011). An improved K-means clustering algorithm. In *2011 IEEE 3rd International Conference on Communication Software and Networks* (pp. 44–46).: The Institute of Electrical and Electronics Engineers.
- Yao, F., Müller, H.-G., & Wang, J.-L. (2005). Functional data analysis for sparse longitudinal data. *Journal of the American Statistical Association*, 100(470), 577–590.
- Yao, Z., Dai, W., & G. Genton, M. (2020). Trajectory functional boxplots. *Stat*, 9(1), e289.
- Zambelli, A. E. (2016). A data-driven approach to estimating the number of clusters in hierarchical clustering. *F1000Research*, 5.
- Zhou, S., Xu, Z., & Liu, F. (2016). Method for determining the optimal number of clusters based on agglomerative hierarchical clustering. *IEEE Transactions on Neural Networks and Learning Systems*, 28(12), 3007–3017.